Relativistic many-body calculations of the oscillator strengths, transition rates and polarizabilities in Zn-like ions

2010 J. Phys. B: At. Mol. Opt. Phys. 43 074025

(http://iopscience.iop.org/0953-4075/43/7/074025)

J. Phys. B: At. Mol. Opt. Phys. **43** (2010) 074025 (15pp) doi:10.1088/0953-4075/43/7/074025

Relativistic many-body calculations of the oscillator strengths, transition rates and polarizabilities in Zn-like ions

U I Safronova[1] **and M S Safronova**[2]

[1] Physics Department, University of Nevada, Reno, NV 89557, USA and Institute of Spectroscopy, Russian Academy of Science, Troitsk, Moscow, Russia
[2] Department of Physics and Astronomy, 217 Sharp Lab, University of Delaware, Newark, DE 19716, USA

Received 24 August 2009, in final form 21 November 2009
Published 19 March 2010
Online at stacks.iop.org/JPhysB/43/074025

Abstract
Transition rates, oscillator strengths and line strengths are calculated for electric-dipole (E1) transitions between even-parity $4s^2$, $4p^2$, 4s4d, $4d^2$, 4p4f and $4f^2$ states and odd-parity 4s4p, 4s4f, 4p4d and 4d4f states in Zn-like ions with the nuclear charges ranging from $Z = 32$ to 100. Relativistic many-body perturbation theory (RMBPT), including the Breit interaction, is used to evaluate retarded E1 matrix elements in length and velocity forms. The calculations start from a $1s^22s^22p^63s^23p^63d^{10}$ Dirac–Fock potential. First-order RMBPT is used to obtain intermediate coupling coefficients and second-order RMBPT is used to calculate transition matrix elements. Contributions from negative-energy states are included in the second-order E1 matrix elements to ensure the gauge independence of transition amplitudes. Transition energies used in the calculation of oscillator strengths and transition rates are from second-order RMBPT. Ground state scalar $\alpha_0(4s^2\,{}^1S_0)$ polarizabilities are calculated for Zn-like ions from $Z = 33$ to 100. To evaluate the $\alpha_0(4s^2\,{}^1S_0)$ polarizabilities, we calculate RMBPT energies for the odd-parity $4l5l'$ *complex* with $J = 1$ and line strengths between the even-parity $4l4l'$ *complex* with $J = 0$ and the odd-parity $4l5l'$, $4l6l'$ *complexes* with $J = 1$.

(Some figures in this article are in colour only in the electronic version)

1. Introduction

The group II-like elements are presently of significant interest to various AMO fields owing to the development of atomic clocks with various group II atoms (Sr, Hg, Yb, etc). In fact, $5s^2\,{}^1S_0$–$5s5p\,{}^3P_0$ transition frequency in ^{88}Sr has been recommended as the secondary representation of a SI second by the International Committee for Weights and Measures (CIPM) [1]. These atoms have also become of recent interest to quantum information [2]. These applications require good knowledge of atomic properties, such as transition rates and polarizabilities. For example, atomic clock schemes are subject to the blackbody radiation shift that is very hard to measure and needs to be calculated. Quantum information proposals require knowledge of wavelengths where atomic dynamic polarizabilities of group II atoms are zero. Study of degenerate quantum gases requires understanding of the long-range interaction coefficients. New methods for studying group II atoms are currently under development [3]. The main problem faced when developing a novel high-precision method for group II atoms is the lack of benchmark experimental data and comprehensive analysis and comparison of theory and experiment. While second-order relativistic many-body perturbation theory (RMBPT) is not sufficiently precise for accurate prediction of the required properties of neutral systems for some of the applications, it is quite precise for the ions of the corresponding isoelectronic sequence. The second-order calculations allow us to study possible issues that may arise when perturbation theory is combined with other methods, such as configuration interaction (CI) to produce more accurate results [4]. Second-order calculations also give the initial approximation for more accurate coupled-cluster approaches [5]. Zn-like systems are of particular interest owing to the convergence issues of the all-order methods [5]

due to large d-shell excitations. The goal of the present study is to fill gaps in our understanding of Zn-like ion properties and to analyse existing results for our better understanding of the properties of group II atoms in general. Our results are compared extensively with other calculations and experiment where available.

Recently, the relativistic configuration-interaction (CI) method with the numerical Dirac–Fock wavefunctions generated in the field of *ab initio* screened model potential was used by Glowacki and Migdalek [6] to compute oscillator strengths for the spin-allowed and spin-forbidden $4s^2\ ^1S_0$–$4s4p\ ^{1,3}P_1$ transitions in neutral zinc. Lifetimes of the $4s4p\ ^{1,3}P_1$ levels in Ga II were evaluated using the CIV3 code by McElroy and Hibbert in [7]. The CIV3 code includes extensive CI calculations. Relativistic effects were introduced via the Breit–Pauli Hamiltonian. Core polarization effects were included by means of explicit CI [7]. Flexible Atomic Code (FAC) was used recently in [8] to calculate energy levels, oscillator strengths and electron impact collision strengths for Ge-, Ga-, Zn-, Cu-, Ni- and Co-like Au ions. The wavelengths and transition probabilities for EUV and x-ray lines in the spectra from Yb^{40+} to U^{62+} along the zinc isoelectronic sequence were calculated by Quinet *et al* [9]. The multiconfiguration Dirac–Fock (MCDF) model was used. Results were reported for the $4s^2$–$4s4p$, $4s4p$–$4p^2$ and $4s4p$–$4s4d$ transitions [9]. Relativistic many-body calculations of the energies of $n = 4$ states along the zinc isoelectronic sequence were recently reported by Blundell *et al* [10]. The GRASP92 multi-configuration Dirac–Hartree–Fock package was recently [11] employed to calculate excitation energies, ionization potentials and oscillator strengths for all neutral and up to five times ionized species of element Cp, $Z = 112$. Weighted oscillator strengths in Coulomb and Babushkin gauges for E1 transitions in Zn-like Ga II were recently reported by Jönsson *et al* [12]. The graspVU multiconfiguration Dirac–Hartree–Fock package was used in [12] to evaluate energies, oscillator strengths and lifetime data in Zn-like Ga II. The same package was used in [13] to evaluate rates of forbidden lines within the $4s4p\ ^3P$ term and between this term and the $4s^2\ ^1S_0$ ground state for ions between $Z = 30$ (Zn) and $Z = 47$ (Ag^{17+}). Multipole (E1, M1, E2 and M2) transition rates were calculated for the $^1S_0$–$^{1,3}P_1$ electric-dipole, $^1S_0$–$^3P_2$ magnetic-quadrupole and ^3P_J–$^3P_{J'}$ magnetic-dipole and electric-quadrupole transitions [13]. The GRASP2k multiconfiguration Dirac–Hartree–Fock package was used recently in [14] to study the hyperfine interaction-dependent $4s4p\ ^3P_2$ lifetimes in Zn-like ions. A number of publications have been devoted to the investigation of hyperfine interactions in these ions [15–18] within the past 10 years. Hyperfine quenching of the $4s4p\ ^3P_0$ level in Zn-like ions was investigated by Marques *et al* in [17]. The graspVU multiconfiguration Dirac–Hartree–Fock package was used in [16] to calculate transition rates between the $4s4f\ ^3F_{2,3}$ and $4s4d\ ^3D_2$ hyperfine levels in Ga II. It was pointed out in [16] that the hyperfine interaction redistributes the intensity among the hyperfine transitions. The authors underlined that those results have never been reported before and this could be of interest in the ongoing studies of the Ga abundance analysis of peculiar HgMn stars [16].

Oscillator strengths [19–49] and lifetimes [50–68] in Zn-like sequences have been studied in a number of works. Atomic spectra in Zn-like ions were studied in different scientific centres during the last 30 years [69–83]. However, very few papers contain any values for polarizabilities of Zn-like ions [84–89]. Recently, determination of polarizabilities and lifetimes for the Mg, Zn, Cd and Hg isoelectronic sequences was presented by Reshetnikov *et al* in [89]. It was underlined in that work that the measurement of the the lowest resonance transition lifetime can be used to determine the polarizabilities and, alternatively, measurements of the polarizabilities can be used to deduce lifetimes. Additionally, isoelectronic regularities in line strengths can be used to obtain a comprehensive database from a small number of precision lifetime determinations. These methods were applied in [89] to produce values for polarizabilities and lifetimes for the Mg, Zn, Cd and Hg isoelectronic sequences.

In the present paper, an RMBPT method is used to calculate transition rates and oscillator strengths between the $4s^2$, $4p^2$, $4d^2$, $4f^2$, $4s4d$ and $4p4f$ even-parity states and the $4s4p$, $4s4f$, $4p4d$ and $4d4f$ odd-parity states of the zinc isoelectronic sequence for a broad range of the nuclear charge, $Z = 32$–100. RMBPT calculations are based on the Dirac–Fock basis set, and our first-order RMBPT gives results equal to results obtained by MCDF codes. The second-order RMBPT gives us results beyond the MCDF approach. This method was used previously to evaluate oscillator strength and transition rates in Be-, Mg-, Ca- and Yb-like ions in [90–93]. Additionally, we calculate ground state scalar $\alpha_0(4s^2\ ^1S_0)$ polarizabilities for Zn-like ions ($Z = 33$–100). These calculations involve new calculations of RMBPT energies for the odd-parity $4l5l'$ *complex* with $J = 1$ and line strengths between the even-parity $4l4l'$ *complex* with $J = 0$ and the odd-parity $4l5l'$, $4l6l'$ *complexes* with $J = 1$.

In summary, this work presents both a systematic calculation of the transition probabilities between excited states in Zn-like ions and a study of the importance of the correlation corrections to those properties. The final results are used to calculate oscillator strengths, transition rates and polarizabilities to provide benchmark values for Zn-like ions. Our data are compared with the existing measurements.

2. Method

The first-order reduced dipole matrix element $Z^{(1)}$ for the transition between two states $vw(J)$–$v'w'(J')$ [90] is given by

$$Z^{(1)}[v_1w_1(J) - v_2w_2(J')] = \sqrt{[J][J']}\sum_{vw}\sum_{v'w'} S^J(v_1w_1, vw)S^{J'}(v_2w_2, v'w') \times (-1)^{1+j_w+j_{v'}} \begin{Bmatrix} J & J' & 1 \\ j_{v'} & j_w & j_v \end{Bmatrix} Z_{v'w}\delta_{vw'}, \quad (1)$$

where $[J] = 2J+1$. The quantity $\mathcal{S}^J(v_1w_1, vw)$ is a symmetry coefficient defined by

$$\mathcal{S}^J(v_1w_1, vw) = \eta_{v_1w_1}\left[\delta_{v_1v}\delta_{w_1w} + (-1)^{j_v+j_w+J+1}\delta_{v_1w}\delta_{w_1v}\right], \quad (2)$$

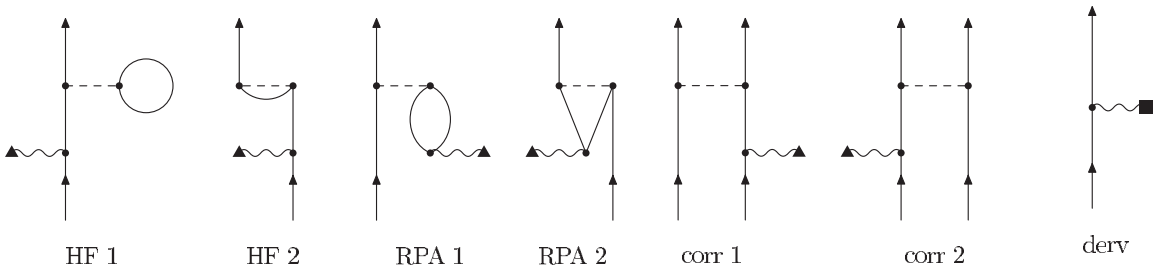

Figure 1. Second-order diagrams for electric-dipole matrix elements.

Table 1. Contributions to E1 uncoupled reduced matrix elements (au) in length L and velocity V forms for transitions between excited states $vw(J)$ and $v'w'(J')$ in Ag^{17+}.

			Coulomb interaction				Coulomb–Breit interaction with factor 10^2			
$vw(J)$	$v'w'(J')$		$Z^{(1)}$	$P^{(\mathrm{derv})}$	$Z^{(\mathrm{RPA})}$	$Z^{(\mathrm{corr})}$	$B^{(\mathrm{HF})}$	$B^{(\mathrm{RPA})}$	$B^{(\mathrm{corr})}$	$B^{(2)}$
$4s_{1/2}4s_{1/2}(0)$	$4s_{1/2}4p_{1/2}(1)$	(L)	0.652 10	0.652 11	−0.032 63	0.009 89	0.050 32	−0.000 79	0.000 26	0.049 78
		(V)	0.650 93	0.000 03	−0.028 80	0.004 05	0.229 87	−0.001 06	−0.00752	0.22130
$4s_{1/2}4s_{1/2}(0)$	$4s_{1/2}4p_{3/2}(1)$	(L)	−0.928 83	−0.928 78	0.045 84	−0.014 07	−0.059 41	0.001 24	−0.000 56	−0.058 72
		(V)	−0.922 02	0.000 08	0.035 75	−0.000 79	−0.058 00	−0.004 58	0.003 05	−0.059 53
$4s_{1/2}4s_{1/2}(0)$	$4p_{1/2}4d_{3/2}(1)$	(L)	0.0	0.0	0.0	0.004 59	0.0	0.0	0.000 71	0.000 71
		(V)	0.0	0.0	0.0	0.001 45	0.0	0.0	0.000 05	0.000 05
$4s_{1/2}4s_{1/2}(0)$	$4p_{3/2}4d_{3/2}(1)$	(L)	0.0	0.0	0.0	−0.002 03	0.0	0.0	−0.000 22	−0.000 22
		(V)	0.0	0.0	0.0	−0.000 50	0.0	0.0	0.001 03	0.001 03
$4s_{1/2}4s_{1/2}(0)$	$4p_{3/2}4d_{5/2}(1)$	(L)	0.0	0.0	0.0	−0.006 50	0.0	0.0	−0.000 97	−0.000 97
		(V)	0.0	0.0	0.0	−0.001 73	0.0	0.0	−0.000 08	−0.000 08
$4s_{1/2}4s_{1/2}(0)$	$4d_{3/2}4f_{5/2}(1)$	(L)	0.0	0.0	0.0	−0.000 13	0.0	0.0	0.000 39	0.000 39
		(V)	0.0	0.0	0.0	0.001 41	0.0	0.0	0.001 01	0.001 01
$4s_{1/2}4s_{1/2}(0)$	$4d_{5/2}4f_{5/2}(1)$	(L)	0.0	0.0	0.0	−0.000 07	0.0	0.0	0.000 01	0.000 01
		(V)	0.0	0.0	0.0	0.000 31	0.0	0.0	0.000 50	0.000 50
$4s_{1/2}4s_{1/2}(0)$	$4d_{5/2}4f_{7/2}(1)$	(L)	0.0	0.0	0.0	−0.000 29	0.0	0.0	0.000 11	0.000 11
		(V)	0.0	0.0	0.0	0.001 63	0.0	0.0	0.000 84	0.000 84

where η_{vw} is a normalization factor given by

$$\eta_{vw} = \begin{cases} 1 & \text{for} \quad w \neq v \\ 1/\sqrt{2} & \text{for} \quad w = v. \end{cases}$$

The second-order reduced matrix element $Z^{(2)}$ for the transition between two states $vw(J)$–$v'w'(J')$ consists of four contributions: Dirac–Hartree–Fock $Z^{(\mathrm{HF})}$ term, random-phase approximation $Z^{(\mathrm{RPA})}$ term, correlation contribution $Z^{(\mathrm{corr})}$ term and derivative $P^{(\mathrm{derv})}$ term [90]. The $Z^{(\mathrm{HF})}$, $Z^{(\mathrm{RPA})}$, $Z^{(\mathrm{corr})}$ and $P^{(\mathrm{derv})}$ contributions to second-order matrix elements in terms of Brueckner–Goldstone diagrams are illustrated in figure 1. The dashed lines indicate Coulomb + Breit interactions and the wavy lines indicate the interaction with the dipole field. Diagrams 'HF 1' and 'HF 2' as well as diagrams 'RPA 1' and 'RPA 2' represent direct and exchange contributions. These diagrams account for the shielding of the dipole field by the core electrons. Diagrams 'corr 1' and 'corr 2' are direct and exchange correlation contributions. These diagrams correct the matrix element to account for the interaction between the valence electrons. The 'derv' diagram represents symbolically the second-order RMBPT correction from the derivative term [90]. A detailed discussion of these diagrams for divalent systems was given by Safronova *et al* [90].

All of the second-order correlation corrections that we discussed above result from the residual Coulomb interaction. To include correlation corrections due to the Breit interaction, the Coulomb matrix element $X_k(abcd)$ (see for detail [94]) must be modified according to the rule

$$X_k(abcd) \rightarrow X_k(abcd) + M_k(abcd) + N_k(abcd), \qquad (3)$$

where M_k and N_k are magnetic radial integrals defined by equations (A4) and (A5) in [95].

2.1. Uncoupled matrix elements

In table 1, we list values of the first- and second-order contributions to electric-dipole matrix elements $Z^{(1)}$, $Z^{(\mathrm{RPA})}$, $Z^{(\mathrm{corr})}$, and the matrix element of the derivative term $P^{(\mathrm{derv})}$ for the $4s_{1/2}4s_{1/2}(0)$–$4l_j4l'_{j'}(1)$ transitions in Zn-like silver, $Z = 47$. Both length and velocity forms of the matrix elements are given. The Coulomb second-order contribution $Z^{(\mathrm{HF})}$ vanishes in the present calculation since we use DF basis functions. We use symbol B in table 1 to denote the Coulomb–Breit contributions to the second-order matrix elements, and we tabulate $100 \times B^{(\mathrm{HF})}$, $100 \times B^{(\mathrm{RPA})}$, $100 \times B^{(\mathrm{corr})}$ and the totals $100 \times B^{(2)}$. We multiply Coulomb–Breit values by 100 for more transparent comparison with Coulomb data. The ratios of the second-order $Z^{(\mathrm{RPA})}$ and the lowest $Z^{(1)}$ contribution are about 5% for the $4s_{1/2}4s_{1/2}(0)$–$4s_{1/2}4p_j(1)$ transitions. However, the other second-order $Z^{(\mathrm{corr})}$ term decreases the ratios of the second and first orders to 3%. The total second-order Breit corrections $B^{(2)}$ also decrease the value of the second-order contribution; however, the ratios of the $B^{(2)}$ and $Z^{(1)}$ terms are very small (about 0.1%).

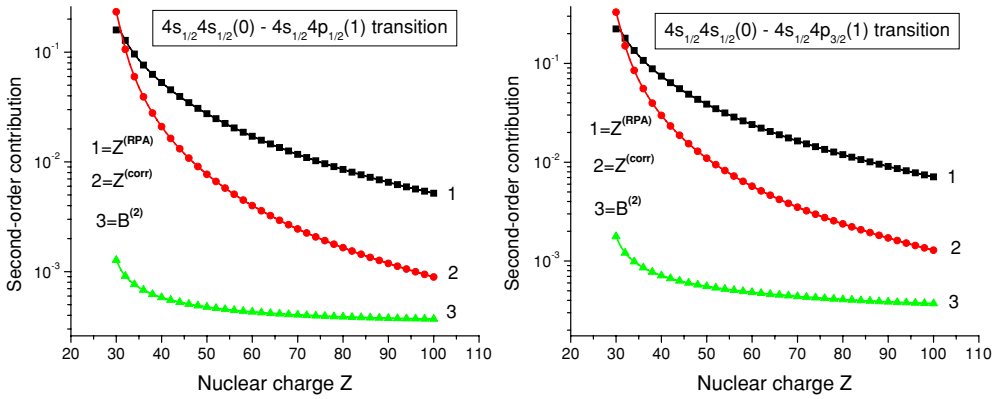

Figure 2. Second-order contributions for electric-dipole matrix elements in Zn-like ions as functions of Z.

The ratios between these terms change with a nuclear charge as illustrated by figure 2 where second-order contributions $Z^{(\mathrm{RPA})}$, $Z^{(\mathrm{corr})}$ and $B^{(2)}$ are shown as functions of Z for the $4s_{1/2}4s_{1/2}(0)$–$4s_{1/2}4p_{1/2}(1)$ and $4s_{1/2}4s_{1/2}(0)$–$4s_{1/2}4p_{3/2}(1)$ electric-dipole matrix elements. The values of the $Z^{(\mathrm{corr})}$ and $Z^{(\mathrm{RPA})}$ terms have different signs and almost cancel each other for low-Z ions. The ratio of these terms decreases very rapidly with Z and becomes 50% for $Z = 37$ and 2% for $Z = 74$. The ratio of the $B^{(2)}$ and $Z^{(\mathrm{RPA})}$ terms slowly increases with Z from 1% for $Z = 37$ and 3% for $Z = 74$.

It should be noted that only the $Z^{(\mathrm{corr})}$ terms are non-zero for two-particle transitions such as the $4s_{1/2}4s_{1/2}(0)$–$4p_j4d_{j'}(1)$ and $4s_{1/2}4s_{1/2}(0)$–$4d_j4f_{j'}(1)$ ones (see table 1). The values of $Z^{(\mathrm{corr})}$ terms for two-particle transitions are of the same order of magnitude as for the one-particle transitions (for example, the $4s_{1/2}4s_{1/2}(0)$–$4s_{1/2}4p_{1/2}(1)$ and $4s_{1/2}4s_{1/2}(0)$–$4p_{3/2}4d_{5/2}(1)$ transitions).

2.2. *Coupled matrix elements*

As mentioned above, physical two-particle states are the linear combinations of uncoupled two-particle states. For the Ag^{17+} example discussed above, the transition amplitudes between physical states are the linear combinations of the uncoupled transition matrix elements given in table 1. The mixing coefficients and energies are obtained by diagonalizing the first-order effective Hamiltonian which includes both Coulomb and Breit interactions. We let $C_1^{\lambda}(av)$ designate the λth eigenvector of the first-order effective Hamiltonian and let E_1^{λ} be the corresponding eigenvalue. The coupled transition matrix element between the initial eigenstate I with the angular momentum J and the final state F with the angular momentum J' is given by

$$
\begin{aligned}
&Q^{(1+2)}(I-F)\\
&\quad=\frac{1}{E_1^I-E_1^F}\sum_{vw}\sum_{v'w'}C_1^I(vw)C_1^F(v'w')\big\{[\epsilon_{vw}-\epsilon_{v'w'}]\\
&\qquad\times[Z^{(1+2)}[vw(J)-v'w'(J')]+B^{(2)}[vw(J)-v'w'(J')]]\\
&\qquad+\big[E_1^I-E_1^F-\epsilon_{vw}+\epsilon_{v'w'}\big]P^{(\mathrm{derv})}[vw(J)-v'w'(J')]\big\}.
\end{aligned}
\tag{4}
$$

Here, $\epsilon_{vw}=\epsilon_v+\epsilon_w$, $Z^{(1+2)}=Z^{(1)}+Z^{(\mathrm{RPA})}+Z^{(\mathrm{corr})}$ and $B^{(2)}=B^{(\mathrm{HF})}+B^{(\mathrm{RPA})}+B^{(\mathrm{corr})}$. Using these formulae together with the uncoupled reduced matrix elements given in table 1, we transform the uncoupled matrix elements to matrix elements between coupled (physical) states.

Values of *coupled* reduced matrix elements in length and velocity forms are given in table 2 for the transitions considered in table 1. Although we use an intermediate-coupling scheme, it is nevertheless convenient to label the physical states using the LS scheme. Both designations are given in table 2. We see that L and V forms of the coupled matrix elements in table 2 differ by only 0.2–0.6%. These L–V differences arise because we start our RMBPT calculations using a non-local Dirac–Fock (DF) potential. If we were to replace the DF potential by a local potential, the differences would disappear completely. The first two columns in table 2 show L and V values of *coupled* reduced matrix elements calculated without the second-order contribution. As we see from this table, removing the second-order contribution increases the $L-V$ differences up to 1–9%.

We used second-order RMBPT code to calculate uncoupled and coupled reduced matrix elements for Zn-like ions given in tables 1 and 2. Unfortunately, the implementation of the third-order RMBPT for heavier systems leads to many problems connected with the intruder states. Therefore, we studied the convergence of the RMBPT approach on the example of Cu-like ions using the RMBPT code developed by Johnson and Savukov [96]. In table 3, we illustrate our results for reduced matrix elements of Cu-like ions with nuclear charge $Z = 36$–100. The first three columns list values obtained in first-, second- and third-order RMBPT for the $4s$–$4p_j$ transitions in Cu-like ions. The fourth and fifth columns show ratios (in %) of the second- and first-order results and the third- and first-order results, respectively. We find that the third-order contribution is less than the second-order contribution by a factor of 5–10. The third-order contributes less than 1% for all of these ions confirming good convergence of RMBPT for Cu-like ions. We find that the ratios of second and first-order results ($Z^{(2)}/Z^{(1)}$) for the Zn-like ions are similar to the ratios shown in the table for Cu-like ions. Therefore, we expect that our conclusion regarding the convergence of MBPT holds for Zn-like ions as well.

Table 2. Coupled reduced matrix elements Q calculated in length L and velocity V forms for Ag^{17+}.

		First order		RMBPT			
$l_1 l_2 LSJ$	$l_3 l_4 L'S'J'$	L	V	L	V	$j_1 j_2$ (J)	$j_3 j_4$ (J')
$4s^2\,{}^1S_0$	$4s4p\,{}^3P_1$	0.226 30	0.227 72	0.217 75	0.218 76	$4s_{1/2}4s_{1/2}(0)$	$4s_{1/2}4p_{1/2}(1)$
$4s^2\,{}^1S_0$	$4s4p\,{}^1P_1$	1.030 71	1.024 55	0.992 77	0.996 36	$4s_{1/2}4s_{1/2}(0)$	$4s_{1/2}4p_{3/2}(1)$
$4s^2\,{}^1S_0$	$4p4d\,{}^3D_1$	0.007 59	0.007 66	0.005 26	0.005 28	$4s_{1/2}4s_{1/2}(0)$	$4p_{1/2}4d_{3/2}(1)$
$4p^2\,{}^3P_0$	$4p4d\,{}^1P_1$	0.071 18	0.070 56	0.069 78	0.069 98	$4p_{1/2}4p_{1/2}(0)$	$4p_{3/2}4d_{5/2}(1)$
$4p^2\,{}^1S_0$	$4s4p\,{}^3P_1$	0.093 44	0.091 78	0.087 48	0.087 86	$4p_{3/2}4p_{3/2}(0)$	$4s_{1/2}4p_{1/2}(1)$
$4p^2\,{}^1S_0$	$4s4p\,{}^1P_1$	0.660 94	0.655 63	0.648 67	0.650 74	$4p_{3/2}4p_{3/2}(0)$	$4s_{1/2}4p_{3/2}(1)$
$4p^2\,{}^1S_0$	$4p4d\,{}^3D_1$	0.062 61	0.063 55	0.060 36	0.060 64	$4p_{3/2}4p_{3/2}(0)$	$4p_{1/2}4d_{3/2}(1)$
$4p^2\,{}^1S_0$	$4p4d\,{}^3P_1$	0.031 02	0.031 39	0.029 84	0.029 94	$4p_{3/2}4p_{3/2}(0)$	$4p_{3/2}4d_{3/2}(1)$
$4d^2\,{}^3P_0$	$4s4p\,{}^1P_1$	0.004 60	0.004 57	0.008 38	0.008 35	$4d_{3/2}4d_{3/2}(0)$	$4s_{1/2}4p_{3/2}(1)$
$4d^2\,{}^3P_0$	$4p4d\,{}^1P_1$	0.092 25	0.093 14	0.090 19	0.090 54	$4d_{3/2}4d_{3/2}(0)$	$4p_{3/2}4d_{5/2}(1)$
$4d^2\,{}^3P_0$	$4d4f\,{}^3D_1$	0.886 78	0.907 34	0.877 14	0.882 09	$4d_{3/2}4d_{3/2}(0)$	$4d_{3/2}4f_{5/2}(1)$
$4d^2\,{}^3P_0$	$4d4f\,{}^3P_1$	0.066 50	0.068 30	0.064 66	0.065 10	$4d_{3/2}4d_{3/2}(0)$	$4d_{5/2}4f_{5/2}(1)$
$4d^2\,{}^3P_0$	$4d4f\,{}^1P_1$	0.062 82	0.063 79	0.063 85	0.064 11	$4d_{3/2}4d_{3/2}(0)$	$4d_{5/2}4f_{7/2}(1)$
$4d^2\,{}^1S_0$	$4s4p\,{}^3P_1$	0.003 94	0.003 89	0.004 30	0.004 31	$4d_{5/2}4d_{5/2}(0)$	$4s_{1/2}4p_{1/2}(1)$
$4d^2\,{}^1S_0$	$4s4p\,{}^1P_1$	0.015 05	0.016 41	0.017 85	0.017 83	$4d_{5/2}4d_{5/2}(0)$	$4s_{1/2}4p_{3/2}(1)$
$4d^2\,{}^1S_0$	$4p4d\,{}^3D_1$	0.118 35	0.117 22	0.117 16	0.117 60	$4d_{5/2}4d_{5/2}(0)$	$4p_{1/2}4d_{3/2}(1)$
$4d^2\,{}^1S_0$	$4d4f\,{}^3D_1$	0.064 91	0.066 82	0.063 47	0.063 89	$4d_{5/2}4d_{5/2}(0)$	$4d_{3/2}4f_{5/2}(1)$
$4d^2\,{}^1S_0$	$4d4f\,{}^3P_1$	0.005 95	0.006 06	0.005 62	0.005 62	$4d_{5/2}4d_{5/2}(0)$	$4d_{5/2}4f_{5/2}(1)$
$4d^2\,{}^1S_0$	$4d4f\,{}^1P_1$	0.893 07	0.912 97	0.893 27	0.898 05	$4d_{5/2}4d_{5/2}(0)$	$4d_{5/2}4f_{7/2}(1)$
$4f^2\,{}^3P_0$	$4d4f\,{}^3D_1$	0.780 75	0.799 60	0.753 19	0.757 41	$4f_{5/2}4f_{5/2}(0)$	$4d_{3/2}4f_{5/2}(1)$
$4f^2\,{}^3P_0$	$4d4f\,{}^3P_1$	0.192 83	0.197 49	0.191 32	0.192 32	$4f_{5/2}4f_{5/2}(0)$	$4d_{5/2}4f_{5/2}(1)$
$4f^2\,{}^3P_0$	$4d4f\,{}^1P_1$	0.062 22	0.064 01	0.059 91	0.060 27	$4f_{5/2}4f_{5/2}(0)$	$4d_{5/2}4f_{7/2}(1)$
$4f^2\,{}^1S_0$	$4d4f\,{}^3D_1$	0.068 62	0.069 98	0.067 00	0.067 30	$4f_{7/2}4f_{7/2}(0)$	$4d_{3/2}4f_{5/2}(1)$
$4f^2\,{}^1S_0$	$4d4f\,{}^1P_1$	0.850 32	0.870 77	0.816 58	0.820 54	$4f_{7/2}4f_{7/2}(0)$	$4d_{5/2}4f_{7/2}(1)$

Table 3. Correlation correction contributions to the 4s–4p E1 matrix elements of Cu-like ions.

Z	$Z^{(1)}$ (au)	$Z^{(1)}+Z^{(2)}$ (au)	$Z^{(1)}+Z^{(2)}+Z^{(3)}$ (au)	$Z^{(2)}/Z^{(1)}$ (%)	$Z^{(3)}/Z^{(1)}$ (%)
			4s–4p$_{1/2}$ transitions		
36	1.1351	1.0614	1.0512	−6.493	−0.898
40	0.8898	0.8391	0.8341	−5.700	−0.563
50	0.5856	0.5592	0.5577	−4.501	−0.264
60	0.4359	0.4195	0.4188	−3.772	−0.158
70	0.3448	0.3335	0.3332	−3.276	−0.107
80	0.2827	0.2744	0.2742	−2.923	−0.079
100	0.2013	0.1963	0.1962	−2.501	−0.050
			4s–4p$_{3/2}$ transitions		
36	1.6099	1.5063	1.4922	−6.435	−0.878
40	1.2639	1.1926	1.1857	−5.642	−0.546
50	0.8352	0.7982	0.7961	−4.435	−0.250
60	0.6250	0.6019	0.6010	−3.695	−0.146
70	0.4973	0.4815	0.4810	−3.186	−0.096
80	0.4102	0.3987	0.3984	−2.817	−0.068
100	0.2952	0.2883	0.2882	−2.348	−0.041

2.3. Negative-energy contributions

It should be emphasized that we include negative energy state (NES) contributions into the sums over the intermediate states. Ignoring the NES contributions leads only to small changes in the L-form matrix elements but to substantial changes in some of the V-form matrix elements, with a consequent loss of gauge independence for a local potential.

The NES contributions to the second-order reduced matrix elements arise from the terms in the sums over states i and n in the $Z^{(\mathrm{corr})}$ contributions [90] for which single-particle energy $\varepsilon_i < -mc^2$. The NES contributions for relativistically allowed transitions were discussed in [90, 91, 97] for Be-like and Mg-like ions, where they were found to be the most important for velocity-form matrix elements; they do not significantly modify length-form matrix elements. In [90], it was shown that NES contributions can be of the same order of magnitude as the 'regular' positive-energy contributions for certain non-relativistically forbidden transitions in Be-like ions. We observe similar large contributions for LS-forbidden transitions here. The matrix elements in tables 1 and 2 include NES contributions.

In figure 3, we illustrate the Z-dependence of the differences between line strengths calculated in length S_L and velocity S_V forms for the $4s^2\,{}^1S_0$–$4s4p\,{}^1P_1$ and $4s^2\,{}^1S_0$–$4s4p\,{}^3P_1$ transitions. We plot the ratio $(S_L-S_V)/S_L$ (in %)

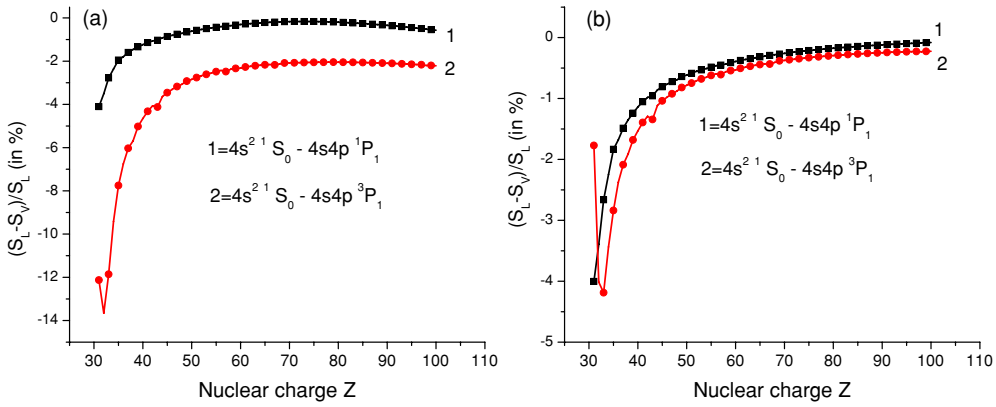

Figure 3. Difference between the values of line strengths calculated in length (S_L) and velocity (S_V) gauges for E1 transitions in Zn-like ions as functions of Z. Graph (a) shows data without NES contributions and graph (b) shows data with NES contributions.

calculated without (a) and with (b) negative-energy state contributions to the second-order reduced matrix elements. The ratio $(S_L - S_V)/S_L$ for the $4s^2\,{}^1S_0$–$4s4p\,{}^1P_1$ transition decreases from 1.2% for $Z = 40$ to 0.17% for $Z = 70$, respectively. The ratio $(S_L - S_V)/S_L$ for the $4s^2\,{}^1S_0$–$4s4p\,{}^3P_1$ transitions decreases from 4.7% for $Z = 40$ to 2.1% for $Z = 70$. However, this ratio decreases substantially (from 1.5% for $Z = 40$ to 0.37% for $Z = 70$) when NES are included for the $4s^2\,{}^1S_0$–$4s4p\,{}^3P_1$ transition. No large changes with including NES are observed in the $(S_L - S_V)/S_L$ ratio for the $4s^2\,{}^1S_0$–$4s4p\,{}^1P_1$ transition (see the right panel of figure 3).

In view of the gauge dependence issue discussed above, our results below are presented in the L form to decrease the volume of tabulated material. Uncertainties in the recommended values given in [98] were estimated to be less than 10% based on comparisons with experimental results from lifetime and emission measurements. The agreement between theoretical L-form and V-form results was also used in [98] as an indicator of accuracy. Since the present transition data are obtained using a single method for all Z and improves in accuracy with increasing Z, owing to the decrease of relative importance of correlation correction, we expect our data for high Z to be very reliable.

3. Results and discussion

We calculate line strengths, oscillator strengths and transition probabilities for 851 $[4l_14l_2\,{}^{1,3}L_J$–$4l_34l_4\,{}^{1,3}L'_{J'}]$ lines for all ions with $Z = 32$–100. The results were calculated in both length and velocity forms, but only length-form results are presented in the following tables and figures for reasons discussed in the previous section. The theoretical energies used to evaluate oscillator strengths and transition probabilities are calculated using the second-order RMBPT formalism developed in [10].

3.1. Transition rates

The general trends of the Z-dependence of transition rates for the $4l_14l_2\,{}^{1,3}L_J$–$4l_34l_4\,{}^{1,3}L'_{J'}$ lines are presented in figures 4 and 5. In these figures, we show transitions to a fixed J state from states belonging to a limited set of the $4l4l'\,{}^{1,3}L_J$ states, i.e. a *complex* of states. A complex includes all states of the same parity and J obtained from the combinations of the $4l4l'\,{}^{1,3}L_J$ states. For example, the odd-parity complex with $J = 1$ includes the states $4s4p\,{}^{1,3}P_1$, $4p4d\,{}^3D_1$, $4p4d\,{}^{1,3}P_1$, $4d4f\,{}^3D_1$ and $4d4f\,{}^{1,3}P_1$ in LS coupling or $4s_{1/2}4p_{1/2}(1)$, $4s_{1/2}4p_{3/2}(1)$, $4p_{1/2}4d_{3/2}(1)$, $4p_{3/2}4d_{3/2}(1)$, $4p_{3/2}4d_{5/2}(1)$, $4d_{3/2}4f_{5/2}(1)$, $4d_{5/2}4f_{5/2}(1)$ and $4d_{5/2}4f_{7/2}(1)$ in jj coupling. Later, we use the LS designations since they are more conventional.

In the top two panels of figure 4, we present a limited set (11 among 56 transitions included in the even-parity complex with $J = 0$ and odd-parity complexes with $J = 1$) of transition rates for the $4s^2\,{}^1S_0$–$4s4p\,{}^{1,3}P_1$, $4s^2\,{}^1S_0$–$4p4d\,{}^{1,3}P_1$, $4s^2\,{}^1S_0$–$4d4f\,{}^1P_1$, $4p^2\,{}^1S_0$–$4s4p\,{}^{1,3}P_1$, $4p^2\,{}^1S_0$–$4p4d\,{}^{1,3}P_1$ and $4p^2\,{}^1S_0$–$4d4f\,{}^{1,3}P_1$ transitions. It should be noted that only two transitions shown in the left top panel of figure 4 (curves '1' and '2') are the 4s–4p electric-dipole one-particle transitions. Other three transitions (curves '3', '4' and '5') are forbidden as electric-dipole one-particle transitions. The values of transition rates for these transitions are non-zero because of two-particle interaction between the $[4s^2 + 4p^2 + 4d^2 + 4f^2]$ and [4s4p + 4p4d + 4d4f] configurations as well as because of the second-order contribution from correlation diagrams $Z^{(\mathrm{corr})}$ as demonstrated in table 1. As a result, the transition rates of these two-particle $4s^2\,{}^1S_0$–$4p4d\,{}^{1,3}P_1$ and $4s^2\,{}^1S_0$–$4d4f\,{}^1P_1$ transitions presented in the left top panel of figure 4 are smaller (by two to four orders of magnitude) than the transition rates of one-particle $4s^2\,{}^1S_0$–$4s4p\,{}^{1,3}P_1$ lines for small Z but become even larger for high Z. Similar ratios between the allowed $4p^2$–4p4d electric-dipole one-particle transitions and the forbidden $4p^2$–4d4f electric-dipole two-particle transitions are demonstrated by the top right panel of figure 4.

In the bottom two panels of figure 4, we present a limited set of transition rates for the 4s4d–4p4d, $4p^2$–4p4d, 4s4d–4s4f and $4p^2$–4s4f transitions (12 among 250 transitions between the states from the odd-parity complex with $J = 2$ and even parity complexes with $J = 1$, 2, and 3). The 4s4d–4p4d and $4p^2$–4p4d transitions are illustrated by the $4s4d\,{}^{1,3}D_J$–$4p4d\,{}^1D_2$ and by $4p^2\,{}^3P_J$–$4p4d\,{}^1D_2$ transitions shown in the bottom left panel of figure 4. In the bottom right

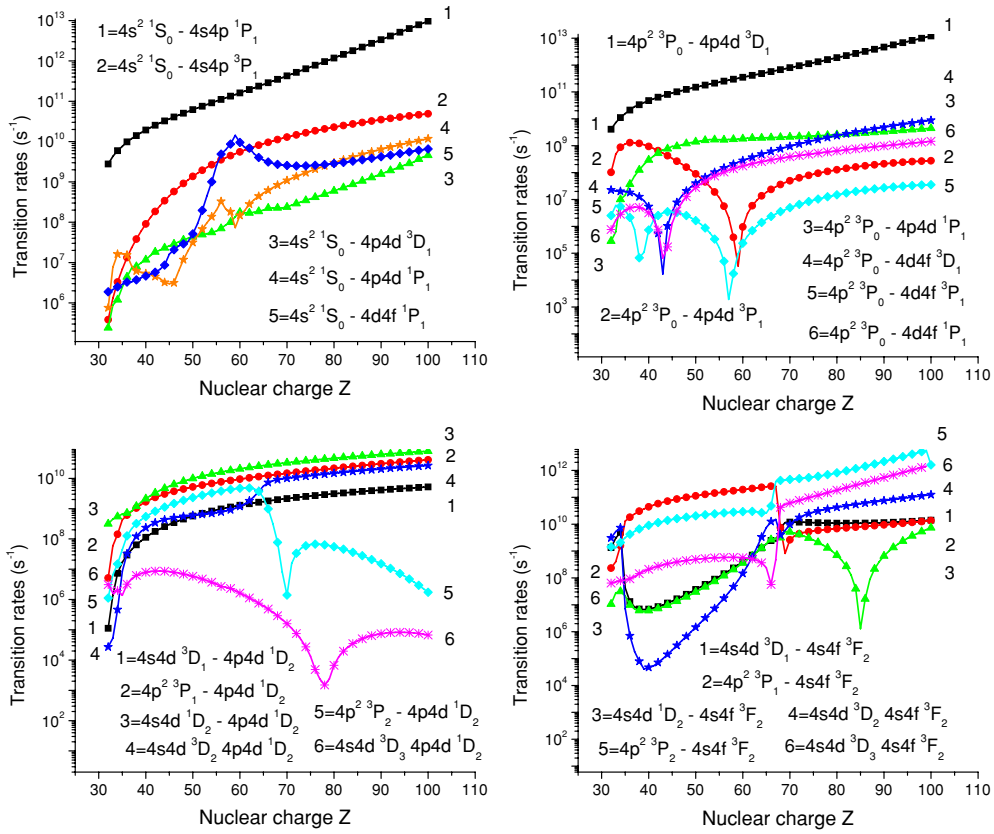

Figure 4. Transition rates for even–odd transitions in Zn-like ions as a function of Z.

panel of figure 4, we show Z dependence of transition rates for the $4s4d\,^{1,3}D_J$–$4s4f\,^3F_2$ and the $4p^2\,^3P_J$–$4s4f\,^3F_2$ transitions.

In the six panels of figure 5, we present all possible 4s4p–4s4d and 4s4p–$4p^2$ electric-dipole one-particle transitions. The smallest values of transition rates are observed in figure 5 for singlet–triplet transitions: curves '2' and '3' (top left panel), curves '3' and '4' (top right panel), curves '2' and '4' (centre left panel), curves '1' and '3' (centre and bottom right panels) and curve '3' (bottom left panel). It should be noted that in some cases this statement is not true for high-Z ions (see, for example, curves '2, 4' and '1, 3' on the centre left panel and curves '1' and '2' on the centre right panel of figure 5).

We see from the graphs that transitions with smooth Z dependences are rarer than transitions with sharp features but they still occur for all transition types: triplet–triplet, singlet–singlet and singlet–triplet, and include transitions with both small J and large J. One general conclusion that can be derived from those graphs is that the smooth Z-dependences occur more frequently for transitions with the largest values of transition rates among the transitions inside complexes.

Singularities in the transition-rate curves have three distinct origins: avoided level crossings, zeros in the dipole matrix elements and zeros in transition energies. Avoided level crossings result in changes of the dominant level configuration at a particular value of Z and lead to abrupt changes in the transition rate curves when the rates associated with the dominant configurations below and above the crossing point are significantly different. Zeros in transition matrix elements as functions of Z lead to cusp-like minima in the transition rate curves. Zeros in transition energies occur at high Z when levels of different parity cross.

Examples of each of these three singularity types are illustrated by figures 4 and 5. Dramatic example of the first type, avoided level crossings, is seen in the bottom right panel of figure 4 at $Z = 68$, corresponding to a change in the dominant configuration for the $4s4f\,^3F_2$ state, the $4p_{3/2}4d_{7/2}(2)$ instead of the $4s_{1/2}4f_{5/2}(2)$ configuration. Examples of the second type, zeros in matrix elements, are seen on the centre left panel of figure 5 at $Z = 61$–62 for the $4s4p\,^3P_1$–$4p^2\,^3P_2$ transition. Finally, singularity of the third type, corresponding to a very small (near zero) transition energy is seen at $Z = 73$ in the top-left panel of figure 5 for the $4s4p\,^1P_1$–$4p^2\,^3P_0$ transition. In this case, the level inversion occur at the interface between the upper even- and odd-parity groups at high Z. The upper $4p^2\,^3P_0$ level becomes the lower $4p^2\,^3P_0$ level; however, the lower $4s4p\,^1P_1$ level becomes the upper level at $Z = 73$.

3.2. Wavelengths, transition rates and oscillator strengths

In tables 4 and 5, wavelengths and electric-dipole transition rates for the 16 $4s^2$–4s4p, 4s4p–4s4d, 4s4p–$4p^2$ transitions in Zn-like ions with $Z = 70$–92 are presented. The RMBPT results are compared with experimental wavelengths from [9]. To save space, we did not include theoretical wavelengths and electric-dipole transition rates for the $4s^2$–4s4p, 4s4p–4s4d, 4s4p–$4p^2$ transitions calculated in [9]. These values were obtained using the fully relativistic

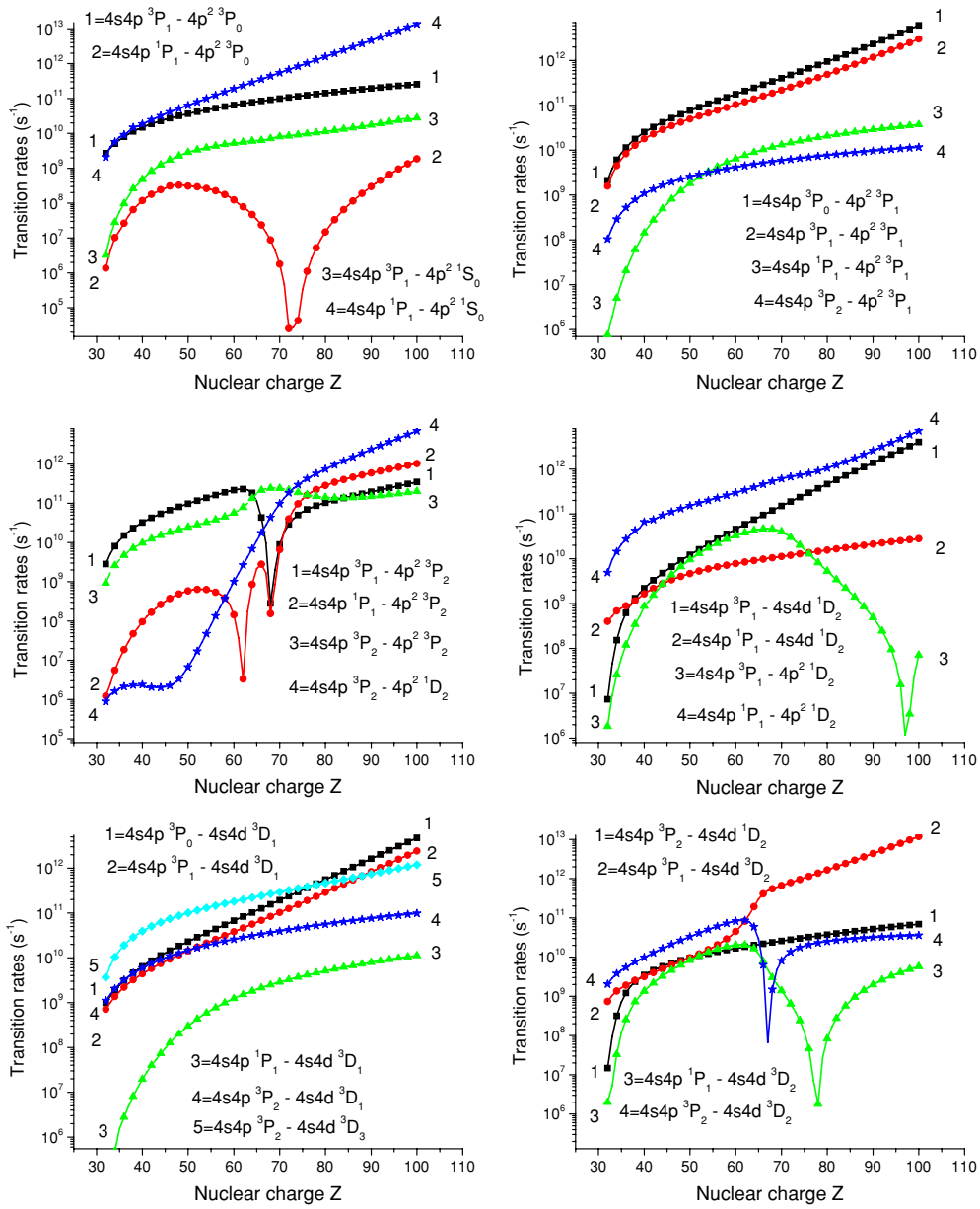

Figure 5. Transition rates for odd–even transitions in Zn-like ions as a function of *Z*.

multiconfiguration Dirac–Fock (MCDF) approach with the latest version of GRASP (General-purpose Relativistic Atomic Structure Package). The $4l4l'$ model space was used for most of the ions, and $4l5l'$ model space was added for Yb XLI and U LXIII [9]. This expansion of the model space resulted in only small differences in the results. The wavelengths were modified on average by only 0.012% and 0.009% while the changes of transition probabilities ranged from 0.60% to 0.70% in these two ions, respectively. We made detailed comparison with results from [9] and confirmed that our first-order RMBPT transition rates are in excellent agreement with transition rates from [9] (since similar model spaces are used). The second-order RMBPT includes additional correlation effects beyond the MCDF approach and is expected to produce more accurate results.

We find excellent agreement of our RMBPT values of wavelengths with experimental results taking into account experimental uncertainties. It should be noted that experimental values presented in [9] were taken from laboratories using different facilities, resulting in different uncertainties shown in experimental wavelengths listed in tables 4 and 5. The values for the $4s_{1/2}4p_{1/2}(1)$–$4p_{1/2}4p_{3/2}(2)$ and $4s_{1/2}4p_{3/2}(2)$–$4p_{1/2}4p_{3/2}(2)$ transitions in W^{44+} have the smallest uncertainties (0.0062 Å and 0.0040 Å). These measurements were done at the EBIT facility at the Lawrence Livermore National Laboratory [99]. Electron-beam energies of about 3 keV were sufficient to produce ions in all of the charge states of present interest [99]. For most of the wavelengths, the uncertainties were equal to 0.020 Å [79]. The spectra from laser-produced plasmas were recorded using a 3 m grazing incidence spectrograph. Thick planar targets were irradiated by one beam of the Nova laser at the Lawrence Livermore National Laboratory [79]. The uncertainties of

Table 4. Wavelengths (λ in Å) and transition rates (A_r in s^{-1}) for the $4s^2$–4s4p and 4s4p–4s4d transitions in Zn-like ions, $Z = 70$–92. The RMBPT results (RMBPT) are compared with experimental (expt) wavelength results presented in [9]. Subscripts a, b, c and d indicate uncertainties of 0.020 Å, 0.005 Å, 0.050 Å and 0.100 Å, respectively.

Z	RMBPT λ (Å)	expt λ (Å)	RMBPT A_r (s^{-1})	RMBPT λ (Å)	expt λ (Å)	RMBPT A_r (s^{-1})	RMBPT λ (Å)	expt λ (Å)	RMBPT A_r (s^{-1})	RMBPT λ (Å)	expt λ (Å)	RMBPT A_r (s^{-1})
	$4s_{1/2}4s_{1/2}(0)$–$4s_{1/2}4p_{3/2}(1)$			$4s_{1/2}4s_{1/2}(0)$–$4s_{1/2}4p_{1/2}(1)$			$4s_{1/2}4p_{1/2}(1)$–$4s_{1/2}4d_{5/2}(2)$			$4s_{1/2}4p_{1/2}(0)$–$4s_{1/2}4d_{3/2}(1)$		
70	73.790	73.792[a]	4.27[11]	147.949	148.170[d]	1.30[10]	57.561	57.540[a]	6.65[11]	73.457	73.461[a]	1.92[11]
71	70.320	70.317[a]	4.72[11]	143.939		1.38[10]	55.166	55.159[a]	7.27[11]	69.982	69.979[a]	2.14[11]
72	67.067	67.015[a]	5.20[11]	140.303	140.048[b]	1.46[10]	52.884	52.878[a]	7.95[11]	66.728	66.672[a]	2.37[11]
73	63.887	63.869[a]	5.77[11]	136.438		1.56[10]	50.704	50.677[a]	8.70[11]	63.549	63.552[a]	2.64[11]
74	60.906	60.900[a]	6.38[11]	132.928		1.66[10]	48.621	48.604[a]	9.53[11]	60.572	60.581[a]	2.93[11]
75	58.069	58.071[a]	7.06[11]	129.552		1.75[10]	46.629	46.598[a]	1.04[12]	57.741	57.742[a]	3.26[11]
76	55.371	55.384[c]	7.82[11]	126.314		1.85[10]	44.722		1.14[12]	55.050		3.63[11]
77	52.804		8.66[11]	123.205		1.95[10]	42.896		1.26[12]	52.491		4.04[11]
78	50.360		9.60[11]	120.212		2.06[10]	41.147		1.38[12]	50.056		4.49[11]
79	48.033	48.063[a]	1.06[12]	117.333		2.16[10]	39.470	39.453[a]	1.51[12]	47.740	47.728[a]	5.00[11]
80	45.819		1.18[12]	114.563		2.27[10]	37.863		1.66[12]	45.536		5.56[11]
81	43.710		1.31[12]	111.887		2.38[10]	36.322		1.83[12]	43.437		6.19[11]
82	41.701	41.689[a]	1.45[12]	109.309		2.50[10]	34.844	34.819[a]	2.01[12]	41.440		6.88[11]
83	39.789	39.792[a]	1.61[12]	106.823		2.61[10]	33.426	33.413[a]	2.21[12]	39.538	39.511[a]	7.66[11]
84	37.966		1.79[12]	104.417		2.73[10]	32.065		2.43[12]	37.726		8.53[11]
85	36.230		1.99[12]	102.100		2.85[10]	30.760		2.68[12]	36.002		9.49[11]
86	34.577		2.21[12]	99.866		2.98[10]	29.507		2.95[12]	34.359		1.06[12]
87	33.001		2.45[12]	97.694		3.10[10]	28.304		3.25[12]	32.793		1.18[12]
88	31.498		2.72[12]	95.596		3.23[10]	27.149		3.59[12]	31.301		1.31[12]
89	30.066		3.03[12]	93.561		3.36[10]	26.040		3.95[12]	29.878		1.46[12]
90	28.702	28.702[a]	3.36[12]	91.602		3.49[10]	24.976	24.980[b]	4.36[12]	28.523		1.62[12]
91	27.399		3.74[12]	89.690		3.63[10]	23.953		4.82[12]	27.229		1.81[12]
92	26.159	26.157[a]	4.16[12]	87.860		3.76[10]	22.972	22.953[a]	5.32[12]	25.998	26.000[a]	2.01[12]
	$4s_{1/2}4p_{1/2}(1)$–$4s_{1/2}4d_{3/2}(2)$			$4s_{1/2}4p_{1/2}(1)$–$4s_{1/2}4d_{3/2}(1)$			$4s_{1/2}4p_{3/2}(2)$–$4s_{1/2}4d_{5/2}(3)$			$4s_{1/2}4p_{3/2}(2)$–$4s_{1/2}4d_{5/2}(2)$		
70	75.570	75.423[a]	1.51[11]	76.199		1.03[11]	77.460	77.355[a]	2.93[11]	84.387	84.170[a]	8.08[09]
71	71.966	71.804[a]	1.69[11]	72.551		1.13[11]	75.245	75.140[a]	3.06[11]	82.321	82.177[a]	1.10[10]
72	68.590		1.89[11]	69.136		1.25[11]	73.117	73.022[a]	3.21[11]	80.362	80.226[a]	1.35[10]
73	65.294	65.143[a]	2.12[11]	65.799		1.39[11]	71.072	70.967[a]	3.36[11]	78.491	78.319[a]	1.57[10]
74	62.207	62.106[a]	2.37[11]	62.676		1.54[11]	69.104	68.995[a]	3.52[11]	76.706	76.516[a]	1.75[10]
75	59.272		2.66[11]	59.707		1.71[11]	67.208		3.68[11]	74.999		1.92[10]
76	56.483		2.97[11]	56.886		1.90[11]	65.380		3.86[11]	73.363		2.06[10]
77	53.831		3.32[11]	54.205		2.10[11]	63.617		4.04[11]	71.795		2.19[10]
78	51.309		3.72[11]	51.656		2.33[11]	61.915		4.23[11]	70.289		2.30[10]
79	48.911	48.735[a]	4.15[11]	49.232		2.59[11]	60.270	60.167[a]	4.43[11]	68.841		2.41[10]
80	46.631		4.64[11]	46.928		2.88[11]	58.680		4.63[11]	67.448		2.50[10]
81	44.460		5.19[11]	44.735		3.20[11]	57.141		4.85[11]	66.107		2.59[10]
82	42.394	42.206[a]	5.79[11]	42.649		3.55[11]	55.652	55.558[a]	5.08[11]	64.814		2.67[10]
83	40.429	40.232[a]	6.46[11]	40.664		3.95[11]	54.209	54.063[a]	5.32[11]	63.567		2.75[10]
84	38.557		7.21[11]	38.775		4.39[11]	52.812		5.57[11]	62.364		2.82[10]
85	36.777		8.05[11]	36.978		4.88[11]	51.457		5.83[11]	61.203		2.89[10]
86	35.082		8.97[11]	35.268		5.43[11]	50.143		6.11[11]	60.080		2.95[10]
87	33.467		1.00[12]	33.639		6.03[11]	48.868		6.40[11]	58.995		3.01[10]
88	31.929		1.12[12]	32.087		6.71[11]	47.630		6.71[11]	57.944		3.06[10]
89	30.464		1.24[12]	30.610		7.47[11]	46.428		7.03[11]	56.928		3.12[10]
90	29.069		1.38[12]	29.203		8.31[11]	45.260		7.37[11]	55.943		3.17[10]
91	27.738		1.54[12]	27.862		9.24[11]	44.126		7.72[11]	54.989		3.21[10]
92	26.472	26.254[a]	1.72[12]	26.587		1.03[12]	43.023		8.10[11]	54.064		3.26[10]

0.020 Å are equal to measurement accuracies ranging from 0.03% for the Yb^{40+} ion up to 0.08% for the U^{62+} ion.

Wavelengths (λ in Å) and oscillator strengths for the $4s^2\ ^1S_0$–$4s4p\ ^{1,3}P_1$ transitions in Zn-like ions with $Z = 47$–69 are listed in table 6. Results for oscillator strengths are evaluated in first-order and second-order RMBPT. In two last columns of table 6, we show other theoretical values. The multiconfiguration Dirac–Fock (MCDF) technique (Grant code) was used by Biémont [36] to evaluate values presented in column 'MCDF'. The multiconfiguration relativistic random-phase approximation (MCRRPA) approach developed by Huang and Johnson [32, 100, 101] was implemented to evaluate values presented in the column 'f [32]' of table 6. Some years later the same MCRRPA code was extended to calculate oscillator strengths for the $4s^2\ ^1S_0$–$4s4p\ ^{1,3}P_1$ transitions in Zn-like ions for high-Z ions up to $Z = 92$ [39]. However, we can find only one additional result for Tb^{35+} to include in table 6 from [39]. There are no other differences in results given in columns 'f [32]' and 'f [39]' of table 6. In the last column of table 6, we list oscillator strengths

Table 5. Wavelengths (λ in Å) and transition rates (A_r in s^{-1}) for 4s4p–4p^2 transitions in Zn-like ions, $Z = 70$–92. The RMBPT results (RMBPT) are compared with experimental (expt) wavelength results presented in [9]. Subscripts a, b and c indicate uncertainties of 0.020 Å, 0.0062 Å and 0.0040 Å, respectively.

	RMBPT	expt	RMBPT	RMBPT	expt	RMBPT	RMBPT	expt	RMBPT	RMBPT	expt	RMBPT
Z	λ (Å)	λ (Å)	A_r (s^{-1})	λ (Å)	λ (Å)	A_r (s^{-1})	λ (Å)	λ (Å)	A_r (s^{-1})	λ (Å)	λ (Å)	A_r (s^{-1})
	$4s_{1/2}4p_{1/2}(1)$–$4p_{1/2}4p_{3/2}(2)$			$4s_{1/2}4p_{1/2}(0)$–$4p_{1/2}4p_{3/2}(1)$			$4s_{1/2}4p_{1/2}(1)$–$4p_{1/2}4p_{3/2}(1)$			$4s_{1/2}4p_{3/2}(1)$–$4p_{3/2}4p_{3/2}(0)$		
70	53.944		8.90[09]	56.635	56.617[a]	4.02[11]	58.251		2.18[11]	75.565	75.666[a]	5.44[11]
71	51.326		1.84[10]	54.322	54.317[a]	4.37[11]	55.857	55.945[a]	2.36[11]	71.935	71.651[a]	6.05[11]
72	48.906		2.91[10]	52.110	52.096[a]	4.76[11]	53.567		2.55[11]	68.539	68.249[a]	6.72[11]
73	46.642		3.99[10]	49.993	49.950[a]	5.18[11]	51.375		2.76[11]	65.226	64.957[a]	7.49[11]
74	44.533	44.5299[b]	5.04[10]	47.966	47.900[a]	5.63[11]	49.275	49.369[a]	2.99[11]	62.126	61.860[a]	8.33[11]
75	42.552		6.02[10]	46.023		6.14[11]	47.264		3.24[11]	59.182		9.27[11]
76	40.683		6.95[10]	44.162		6.69[11]	45.336		3.52[11]	56.386		1.03[12]
77	38.914		7.82[10]	42.378		7.29[11]	43.489		3.82[11]	53.729		1.15[12]
78	37.234		8.66[10]	40.667		7.95[11]	41.717		4.15[11]	51.205		1.28[12]
79	35.636		9.48[10]	39.026	39.000[a]	8.68[11]	40.018	40.098[a]	4.51[11]	48.805	48.485[a]	1.42[12]
80	34.114		1.03[11]	37.451		9.47[11]	38.388		4.91[11]	46.524		1.59[12]
81	32.662		1.11[11]	35.940		1.04[12]	36.824		5.34[11]	44.354		1.76[12]
82	31.275		1.19[11]	34.490		1.13[12]	35.323	35.366[a]	5.82[11]	42.290		1.97[12]
83	29.950		1.28[11]	33.097	33.081[a]	1.24[12]	33.883	33.919[a]	6.34[11]	40.327	40.008[a]	2.19[12]
84	28.684		1.36[11]	31.760		1.35[12]	32.500		6.92[11]	38.458		2.44[12]
85	27.473		1.45[11]	30.477		1.48[12]	31.174		7.55[11]	36.681		2.71[12]
86	26.314		1.55[11]	29.244		1.62[12]	29.900		8.25[11]	34.989		3.02[12]
87	25.205		1.64[11]	28.060		1.78[12]	28.677		9.02[11]	33.377		3.37[12]
88	24.144		1.75[11]	26.923		1.95[12]	27.503		9.87[11]	31.843		3.75[12]
89	23.128		1.85[11]	25.831		2.14[12]	26.376		1.08[12]	30.381		4.18[12]
90	22.155		1.96[11]	24.781		2.34[12]	25.293	25.313[a]	1.18[12]	28.989		4.66[12]
91	21.223		2.08[11]	23.773		2.57[12]	24.254		1.30[12]	27.662		5.19[12]
92	20.331		2.21[11]	22.805	22.774[a]	2.82[12]	23.256	23.233[a]	1.42[12]	26.400		5.78[12]
	$4s_{1/2}4p_{3/2}(1)$–$4p_{3/2}4p_{3/2}(2)$			$4s_{1/2}4p_{3/2}(2)$–$4p_{1/2}4p_{3/2}(2)$			$4s_{1/2}4p_{3/2}(1)$–$4p_{1/2}4p_{3/2}(2)$			$4s_{1/2}4p_{1/2}(1)$–$4p_{1/2}4p_{1/2}(0)$		
70	75.717	75.320[a]	6.11[11]	76.834		2.41[11]	85.144	85.385[a]	6.62[09]	132.193		9.91[10]
71	72.690	72.661[a]	6.46[11]	74.053		2.31[11]	81.899	82.035[a]	1.95[10]	128.810		1.03[11]
72	69.701	69.634[a]	6.76[11]	71.522		2.18[11]	78.962		3.99[10]	125.720		1.07[11]
73	66.669	66.647[a]	7.06[11]	69.167		2.03[11]	76.240	76.377[a]	6.64[10]	122.442		1.11[11]
74	63.725	63.706[a]	7.37[11]	67.003	66.9301[c]	1.89[11]	73.750	73.840[a]	9.66[10]	119.448		1.16[11]
75	60.854		7.72[11]	64.985		1.76[11]	71.435		1.29[11]	116.559		1.20[11]
76	58.074		8.12[11]	63.089		1.65[11]	69.267		1.61[11]	113.781		1.24[11]
77	55.396		8.59[11]	61.297		1.57[11]	67.221		1.93[11]	111.106		1.29[11]
78	52.825		9.14[11]	59.592		1.50[11]	65.281		2.24[11]	108.524		1.33[11]
79	50.363	50.406[a]	9.79[11]	57.964		1.45[11]	63.431	63.346[a]	2.55[11]	106.035		1.38[11]
80	48.010		1.05[12]	56.405		1.42[11]	61.662		2.85[11]	103.634		1.42[11]
81	45.763		1.14[12]	54.907		1.39[11]	59.965		3.14[11]	101.310		1.47[11]
82	43.620	43.640[a]	1.23[12]	53.465		1.38[11]	58.334		3.44[11]	99.067		1.52[11]
83	41.578	41.590[a]	1.34[12]	52.075		1.37[11]	56.763	56.677[a]	3.73[11]	96.898		1.57[11]
84	39.631		1.47[12]	50.733		1.37[11]	55.248		4.03[11]	94.796		1.62[11]
85	37.778		1.61[12]	49.435		1.38[11]	53.785		4.33[11]	92.767		1.67[11]
86	36.015		1.76[12]	48.180		1.40[11]	52.370		4.63[11]	90.807		1.73[11]
87	34.334		1.93[12]	46.963		1.41[11]	51.001		4.95[11]	88.898		1.78[11]
88	32.734		2.13[12]	45.784		1.44[11]	49.675		5.27[11]	87.052		1.84[11]
89	31.210		2.35[12]	44.640		1.46[11]	48.390		5.60[11]	85.258		1.89[11]
90	29.761		2.59[12]	43.530		1.50[11]	47.143		5.95[11]	83.527		1.95[11]
91	28.379		2.86[12]	42.452		1.53[11]	45.934		6.30[11]	81.837		2.01[11]
92	27.066		3.16[12]	41.405		1.57[11]	44.760		6.67[11]	80.215		2.06[11]

evaluated by the MCRRPA approach that included additional core excitation channels and use of experimental excitation energies [40].

Comparison of oscillator strengths shown in six columns of table 6 shows that the MCDF ('f [36]') results are in good agreement with our first-order results. There is only a small difference between our first-order results and MCRRPA results given in columns 'f [32]' and 'f [39]'. It should be noted that the RMBPT results are smaller than first-order results by 5–7%. Including core excitation channels in the MCRRPA approach decreases oscillator strengths for the $4s^2\ ^1S_0$–$4s4p\ ^1P_1$ transitions and brings those results closer to our RMBPT values with only 2–3% remaining difference. For the $4s^2\ ^1S_0$–$4s4p\ ^3P_1$ transition, the influence of including core excitation channels in MCRRPA approach appears to be very small. There is only 1% difference in all three MCRRPA f values for the $4s^2\ ^1S_0$–$4s4p\ ^3P_1$ transition.

Table 6. Wavelengths (λ in Å) and oscillator strengths for the $4s^2\ ^1S_0$–$4s4p\ ^{1,3}P_1$ transitions in Zn-like ions, evaluated in first and second orders of RMBPT. The RMBPT values of oscillator strengths are compared with other theoretical results (MCDF method) [36] and (MCRRPA method) [32, 39, 40]. Experimental (expt) wavelengths are from [36] : a, and [79] : b.

	RMBPT	expt	RMBPT	First order	MCDF	MCRRPA		
Z	Wavelengths (Å)		f	f	f [36]	f [32]	f [39]	f [40]
			$4s^2\ ^1S_0$–$4s4p\ ^1P_1$ transition					
47	244.685	244.310[a]	1.224	1.338	1.349	1.374	1.373	1.2653
48	230.272	230.045[a]	1.206	1.315	1.325	1.348	1.348	1.2431
49	217.328	216.977[a]	1.187	1.293	1.302			
50	205.089	204.811(40)[b]	1.173	1.272	1.281			
51	193.841	193.604(40)[b]	1.156	1.252	1.270			
52	183.455	183.175(40)[b]	1.140	1.234	1.247			
53	173.646	173.478(40)[b]	1.127	1.217	1.225	1.243	1.242	1.1523
54	164.610	164.398(40)[b]	1.114	1.202	1.209	1.226	1.225	1.1372
55	156.053	155.939(5)[b]	1.104	1.187	1.195	1.210	1.210	1.1247
56	148.103	147.972(10)[b]	1.095	1.174	1.181	1.197	1.196	1.1131
57	140.491	140.531(20)[b]	1.082	1.162	1.169			
58	133.443	133.452(20)[b]	1.070	1.152	1.159			
59	126.871	126.841(10)[b]	1.058	1.142	1.149			
60	120.644	120.597(5)[b]	1.054	1.134	1.141			
61	114.724	114.680[a]	1.050	1.127	1.134			
62	109.137	109.112(20)[b]	1.046	1.121	1.128			
63	103.849	103.832(20)[b]	1.043	1.116	1.123			
64	98.843	98.824(20)[b]	1.040	1.112	1.119			
65	94.098	94.090[a]	1.039	1.109	1.117		1.127	
66	89.599	89.606(20)[b]	1.039	1.108	1.115			
67	85.333	85.311(20)[b]	1.039	1.107	1.114			
68	81.283	81.303(5)[b]	1.040	1.107	1.114			
69	77.442	77.460[a]	1.042	1.108	1.116			
			$4s^2\ ^1S_0$–$4s4p\ ^3P_1$ transition					
47	351.682	351.804[a]	0.0407	0.0436	0.0451	0.0466	0.0466	0.0487
48	333.211	333.513[a]	0.0458	0.0489	0.0505	0.0520	0.0520	0.0540
49	317.072	316.930[a]	0.0508	0.0543	0.0560			
50	301.729	301.713(40)[b]	0.0562	0.0598	0.0615			
51	287.844	287.819(40)[b]	0.0613	0.0654	0.0670			
52	275.184	275.078(40)[b]	0.0665	0.0708	0.0724			
53	263.362	263.335(40)[b]	0.0716	0.0763	0.0779	0.0796	0.0795	0.0799
54	252.625	252.473(40)[b]	0.0766	0.0815	0.0832	0.0848	0.0848	0.0856
55	242.399	242.390(5)[b]	0.0816	0.0867	0.0883	0.0899	0.0899	0.0897
56	233.042		0.0867	0.0916	0.0932	0.0948	0.0948	0.0943
57	224.316	224.300(100)[b]	0.0906	0.0963	0.0979			
58	216.159		0.0943	0.1008	0.1023			
59	208.455		0.0980	0.1051	0.1065			
60	201.344	201.265(5)[b]	0.1015	0.1091	0.1104			
61	194.561		0.1048	0.1128	0.1141			
62	188.197		0.1083	0.1163	0.1175			
63	182.186	182.200(200)[b]	0.1114	0.1195	0.1206			
64	176.504	176.600(200)[b]	0.1142	0.1225	0.1235			
65	171.119		0.1167	0.1252	0.1262		0.1274	
66	166.007	165.953(5)[b]	0.1187	0.1276	0.1286			
67	161.153		0.1212	0.1299	0.1307			
68	156.534	156.487(5)[b]	0.1236	0.1319	0.1327			
69	152.146		0.1257	0.1337	0.1344			

Wavelengths for the $4s^2\ ^1S_0$–$4s4p\ ^{1,3}P_1$ transitions are compared in two columns of table 6. Our RMBPT values are compared with experimental (expt) wavelengths from [36] and [79]. The uncertainties differ by a factor of 20 for some ions. No uncertainties were given in [36]. The difference between our RMBPT and experimental wavelengths is about 0.01–0.05% and below the uncertainties in experimental measurements. We note that the difference between MCDF [36] and experimental wavelengths is about 1%.

3.3. Ground state static polarizabilities in Zn-like ions

The electric-dipole static polarizability α_0 of the level $\|aJ\rangle$ is defined as [102]

$$\alpha_0(aJ) = \frac{2}{3(2J+1)} \sum_n \frac{|\langle aJ\|D\|nJ'\rangle|^2}{E(aJ) - E(nJ')}. \qquad (5)$$

Here, $\langle aJ\|D\|nJ'\rangle$ is the coupled electric-dipole matrix element defined by equation (4) and $E(aJ)$ is the energy of the

Table 7. Contributions to the electric-dipole polarizability of Zn-like krypton in the $4s^2\,{}^1S_0$ ground state.

Level	First order			RMBPT		
$4l'nl\,{}^{1,3}L_1$	ΔE	D	I	ΔE	D	I
$4s4p\,{}^3P_1$	0.5266	0.1113	1.57[−2]	0.5483	0.1065	1.38[−2]
$4s4p\,{}^1P_1$	0.7949	1.7810	2.66[−0]	0.7772	1.7129	2.52[−0]
$4p4d\,{}^3D_1$	2.2644	0.0091	2.46[−5]	2.2852	0.0072	1.51[−5]
$4p4d\,{}^3P_1$	2.2877	0.0009	2.61[−7]	2.3108	0.0002	1.36[−8]
$4p4d\,{}^1P_1$	2.4491	0.0382	3.97[−4]	2.4393	0.0185	9.34[−5]
$4d4f\,{}^3D_1$	4.0879	0.0004	2.84[−8]	4.1223	0.0001	2.45[−9]
$4d4f\,{}^3P_1$	4.0937	0.0002	3.76[−9]	4.1304	0.0001	1.34[−9]
$4d4f\,{}^1P_1$	4.2196	0.0134	2.84[−5]	4.1995	0.0021	6.76[−7]
	$\alpha_0(4s^2\,{}^1S_0, 4) = 2.6765$			$\alpha_0(4s^2\,{}^1S_0, 4) = 2.5306$		
$4s5p\,{}^3P_1$	2.2190	0.0976	2.86[−3]	2.2562	0.1016	3.05[−3]
$4s5p\,{}^1P_1$	2.2382	0.2225	1.47[−2]	2.2740	0.2330	1.59[−2]
$4p5s\,{}^3P_1$	2.6390	0.0094	2.22[−5]	2.6754	0.0102	2.59[−5]
$4p5s\,{}^1P_1$	2.7054	0.0313	2.41[−4]	2.7203	0.0368	3.32[−4]
$4p5d\,{}^3D_1$	3.2613	0.0069	9.66[−6]	3.2947	0.0040	3.21[−6]
$4p5d\,{}^3P_1$	3.3174	0.0056	6.40[−6]	3.3478	0.0029	1.70[−6]
$4p5d\,{}^1P_1$	3.3418	0.0167	5.59[−5]	3.3397	0.0071	9.95[−6]
$4d5p\,{}^3D_1$	3.8892	0.0014	3.26[−7]	4.0009	0.0004	3.27[−8]
$4d5p\,{}^3P_1$	3.9355	0.0020	6.53[−7]	3.9945	0.0004	2.64[−8]
$4d5p\,{}^1P_1$	3.9854	0.0167	4.65[−5]	4.1277	0.0019	5.98[−7]
	$\alpha_0(4s^2\,{}^1S_0, 5) = 0.0180$			$\alpha_0(4s^2\,{}^1S_0, 5) = 0.0193$		
	$\alpha_0(4s^2\,{}^1S_0) = 2.699$			$\alpha_0(4s^2\,{}^1S_0) = 2.555$		

Designations: $\Delta E = E(4s^2\,{}^1S_0) - E(4l'nl\,{}^{(1,3)}L_1)$,
$D = \langle 4s^2\,{}^1S_0 \| D \| 4l'nl\,{}^{(1,3)}L_1\rangle$,
$I = I(4l'nl\,{}^{(1,3)}L_1) = \frac{2}{3}\frac{|\langle 4s^2\,{}^1S_0 \| D \| 4l'nl\,{}^{(1,3)}L_1\rangle|^2}{E(4s^2\,{}^1S_0) - E(4l'nl\,{}^{(1,3)}L_1)}$,
$\alpha_0(4s^2\,{}^1S_0, n) = \sum_{1,3\,Ll'} I(4l'nl\,{}^{(1,3)}L_1)$. All values are in au.

level $|aJ\rangle$. In the case of the $4s^2\,{}^1S_0$ ground state of Zn-like ions, we can rewrite equation (5) as

$$\alpha_0(4s^2\,{}^1S_0) = \frac{2}{3}\sum_n \sum_{1,3\,Ll'} \frac{|\langle 4s^2\,{}^1S_0 \| D \| 4l'nl\,{}^{(1,3)}L_1\rangle|^2}{E(4s^2\,{}^1S_0) - E(4l'nl\,{}^{(1,3)}L_1)}, \quad (6)$$

where the sum over $ll'\,{}^{(1,3)}L_1$ is a sum over all states included in the odd-parity *complex* with $J = 1$. In the case of $n = 4$, that *complex* consists of eight states: $4s4p\,{}^{1,3}P_1$, $4p4d\,{}^3D_1$, $4p4d\,{}^{1,3}P_1$, $4d4f\,{}^3D_1$ and $4d4f\,{}^{1,3}P_1$. In the case of $n = 5$ and 6, the odd-parity *complex* with $J = 1$ includes the following states: $4snp\,{}^{1,3}P_1$, $4pnd\,{}^3D_1$, $4pnd\,{}^{1,3}P_1$, $4dnp\,{}^3D_1$, $4dnp\,{}^{1,3}P_1$, $4dnf\,{}^3D_1$ and $4dnf\,{}^{1,3}P_1$.

In table 7, we list contributions to dipole polarizability of the $4s^2\,{}^1S_0$ ground state in Zn-like krypton. Both first-order and second-order RMBPT values are listed for comparison. The following designations are used in this table:

$$\alpha_0(4s^2\,{}^1S_0, n) = \sum_{1,3\,Ll'} I(4l'nl\,{}^{(1,3)}L_1)$$
$$I(4l'nl\,{}^{(1,3)}L_1) = \frac{2}{3}\frac{|\langle 4s^2\,{}^1S_0 \| D \| 4l'nl\,{}^{(1,3)}L_1\rangle|^2}{(E(4s^2\,{}^1S_0) - E(4l'nl\,{}^{(1,3)}L_1))}. \quad (7)$$

We also use short labels $E(4s^2\,{}^1S_0) - E(4l'nl\,{}^{(1,3)}L_1) = \Delta E$ and $\langle 4s^2\,{}^1S_0 \| D \| 4l'nl\,{}^{(1,3)}L_1\rangle = D$. The largest contribution to the polarizability of the $4s^2\,{}^1S_0$ ground state in Zn-like krypton comes from the $4s^2\,{}^1S_0$–$4s4p\,{}^1P_1$ transition since the value of $I(4s4p\,{}^{(1)}P_1)$ is almost equal to the $\alpha_0(4s^2\,{}^1S_0, 4)$ value (i.e. contribution from 4s4p states). All other $4s^2\,{}^1S_0$–$4l4l'\,{}^{1,3}L_1$ transitions contribute less than 1% to the $\alpha_0(4s^2\,{}^1S_0, 4)$ value. Contributions from the $4s^2\,{}^1S_0$–$4l5l'\,{}^{1,3}L_1$ transitions give the $\alpha_0(4s^2\,{}^1S_0, 5)$ values equal to 0.0180 au and 0.0193 au, in the first and second orders, respectively (see the second line from bottom in table 7). The $\alpha_0(4s^2\,{}^1S_0, 6)$ value (i.e. contribution from $4l6l'$ states) is equal to 0.004 07 au and 0.005 11 au, in the first and second orders, respectively. The $n = 5$ and $n = 6$ contributions are only 0.7% and 0.2% of the $n = 4$ contribution, respectively, i.e. the sum over n converges very fast. Truncating the sum over n in equation (7) to $n = 6$ results in 0.2% numerical accuracy. The final result for the dipole polarizability of the $4s^2\,{}^1S_0$ ground state in Zn-like krypton is given in the last line of table 7. The experimental value of $\alpha_0(4s^2\,{}^1S_0)$ given by Lundeen and Fehrenbach [88] (2.69(4) au) is in agreement with our value (2.699 au) evaluated in the first-order approach. However, our final value, 2.56 au, is lower by 5%. More accurate configuration + all-order calculations [103] that include correlations in the more complete way are needed to resolve the discrepancy.

In table 8, we list dipole polarizabilities of the $4s^2\,{}^1S_0$ ground state in Zn-like ions with $Z = 33$–47. We compare our RMBPT values with theoretical results given in [89]. In that paper, the polarizabilities were calculated using the lifetime measurements for the lowest resonance transition. It was underlined in [89] that, alternatively, measurements of the polarizabilities can be used to deduce lifetimes. Therefore, we include in table 8 our RMBPT results for the lifetimes of the $4s4p\,{}^1P_1$ level and oscillator strengths for the $4s^2\,{}^1S_0$–$4s4p\,{}^1P_1$

Table 8. Electric-dipole polarizability of the $4s^2\,{}^1S_0$ ground state, lifetime of the $4s4p\,{}^1P_1$ level and oscillator strength for the $4s^2\,{}^1S_0$–$4s4p\,{}^1P_1$ transition in Zn-like ions with $Z = 33$–47. Comparison between RMBPT values and theoretical results given in [89]. Columns with (Δ (in %)) labels show difference between RMBPT and [89] values.

	Polarizability (au)			Lifetime (ns)			Oscillator strengths		
Z	RMBPT	[89]	Δ (%)	RMBPT	[89]	Δ (%)	RMBPT	[89]	Δ (%)
33	6.275	6.19(20)	1.4	0.2325	0.23(3)	1.1	1.582	1.558	1.5
34	4.456	4.61(11)	−3.5	0.1677	0.16	4.6	1.568	1.620	−3.3
35	3.350	3.37(8)	−0.6	0.1317	0.126	4.3	1.532	1.560	−1.8
36	2.555	2.70(5)	−5.7	0.1017	0.096(3)	5.6	1.520	1.598	−5.1
37	2.003	2.00(4)	0.1	0.0842	0.084	0.2	1.476	1.468	0.5
38	1.621	1.597(33)	1.5	0.0710	0.071	0.0	1.443	1.429	1.0
39	1.324	1.299(27)	1.9	0.0598	0.061	2.0	1.419	1.394	1.8
40	1.101	1.071(21)	2.7	0.0516	0.052	0.8	1.390	1.362	2.0
41	0.924	0.895(17)	3.1	0.0448	0.046	2.7	1.363	1.334	2.1
42	0.783	0.755(15)	3.6	0.0393	0.040	1.8	1.337	1.307	2.2
43	0.670	0.644(12)	3.9	0.0346	0.035	1.2	1.314	1.282	2.4
44	0.578	0.552(10)	4.5	0.0307	0.031	1.0	1.289	1.260	2.2
45	0.500	0.477(8)	4.6	0.0273	0.028	2.6	1.267	1.238	2.3
46	0.436	0.413(7)	5.3	0.0245	0.025	2.0	1.245	1.216	2.3
47	0.382	0.361(6)	5.5	0.0220	0.022	0.0	1.224	1.199	2.0

transition in Zn-like ions with $Z = 33$–47. We also list the relative differences between our results and those of [89].

We see from table 8 that the largest disagreement (about 5%) between our RMBPT values and results from [89] for relatively low-Z ions is for Zn-like krypton. Since the lifetime value used in [89] was obtained directly from the polarizability measurement of Lundeen and Fehrenbach [88], it is expected that the polarizability value of [89] exactly agrees with the measurement of [88], since it is based directly on this measurement (see also [67]). We already addressed that discrepancy in the previous paragraph. The differences between the polarizability results for remaining relatively low-Z ions ($Z = 33$–39) vary but either within or close to the uncertainties quoted in [89]. Therefore, the agreement for these ions is very good. For higher Z ions, we observe a systematic increase between our polarizability values and that of [89]. We note that all of these higher-Z values are based on extrapolated lifetime data owing to lack of measured data. It would be expected that the accuracy of the extrapolated data decreases for higher Z. However, we find excellent agreement (0–2%) between both results for the lifetime and oscillator strengths shown in this table for Zn-like ions with $Z = 37$–47. Therefore, the systematic increase of the differences between the polarizabilities may be due to the procedure used in [89] to deduce polarizabilities from the lifetime results. This difference may also be due to increased relativistic effects contributing to the $\alpha_0(4s^2\,{}^1S_0)$ polarizability in high-Z ions. Our calculations are intrinsically relativistic, and we expect the accuracy of our values to actually improve for higher Z owing to decreased correlation corrections.

Contribution of relativistic effects is illustrated in figure 6 where we plot electric-dipole polarizabilities of the $4s^2\,{}^1S_0$ ground state in Zn-like ions as functions of Z. Together with the $\alpha_0(4s^2\,{}^1S_0)$ value (curve '3'), we illustrate contributions of two channels: the $4s^2\,{}^1S_0$–$4snp\,{}^1P_1$ and $4s^2\,{}^1S_0$–$4snp\,{}^3P_1$ transitions, where $n = 4$ and 5. Those channels give numerical values for the following terms: $[I(4s4p\,{}^1P_1) + I(4s4p\,{}^1P_1)]$ and $[I(4s4p\,{}^3P_1) + I(4s4p\,{}^3P_1)]$

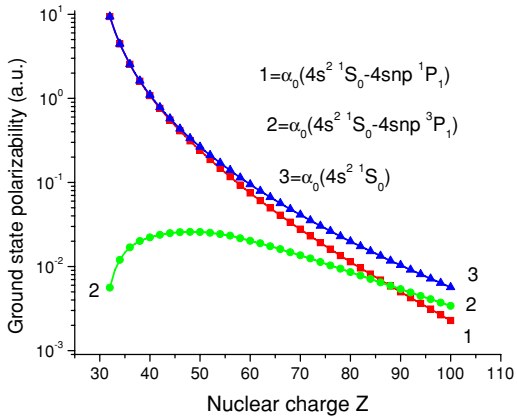

Figure 6. Contribution to dipole polarizability of the $4s^2\,{}^1S_0$ ground state in Zn-like ions as functions of Z.

(see equation (7)), described by curves '1' and '2', respectively. The contribution of $[I(4s4p\,{}^3P_1) + I(4s4p\,{}^3P_1)]$ term increases with Z and for $Z > 87$ even became larger than the $[I(4s4p\,{}^1P_1) + I(4s4p\,{}^1P_1)]$ term. The $[I(4s4p\,{}^3P_1) + I(4s4p\,{}^3P_1)]$ term needs to be included in calculation of the $4s^2\,{}^1S_0$ ground state polarizability in Zn-like ions with $Z > 37$ if we want to guarantee 1% accuracy. That term was not considered in [89].

We already mentioned that the largest contribution to the ground state $4s^2$ polarizabilities in Zn-like ions comes from the 4s–4p one-electron transition $4s^2\,{}^1S_0$–$4s4p\,{}^1P_1$. To estimate the effect of the continuous contributions, we carried out additional calculations of the ground state 4s polarizabilities in Cu-like ions. We find that the continuum contributes less than 0.2–0.3% to the value of the ground state 4s polarizabilities in Cu-like ions. We note that Sr $5s^2$ ground state polarizability has been studied in detail in [104, 105] using a combination of the configuration interaction and many-body perturbation theory. The continuum contribution has been included is those works. The same ($n = 5$) single transition was found to give overwhelmingly dominant contribution to

the polarizability. Replacement of its contribution by the value determined from the precision experiment modified the final result by about 2.5% which exceeds the continuum contribution. Therefore, the main uncertainty in the ground state polarizability calculation comes from the uncertainty in the E1 matrix element for the dominant transition.

4. Conclusion

We have presented a systematic second-order relativistic MBPT study of the reduced matrix elements, oscillator strengths and transition rates for the 4s–4p, 4p–4d, 4d–4f electric-dipole transitions in zinc-like ions with the nuclear charge Z ranging from 33 to 100. Our retarded $E1$ matrix elements include correlation corrections from Coulomb and Breit interactions. Both length and velocity forms of the matrix elements were evaluated, and small differences, caused by the non-locality of the starting DF potential, were found between the two forms. Contributions from negative energy states were also included in order to improve the agreement between results calculated in lengths and velocity gauges. Second-order RMBPT transition energies were used in our evaluation of the oscillator strengths and transition rates. Ground state scalar $\alpha_0(4s^2\ ^1S_0)$ polarizabilities were calculated for Zn-like ions ($Z = 33$–100). To evaluate the $\alpha_0(4s^2\ ^1S_0)$ polarizabilities, we calculate RMBPT energies for the odd-parity $4l5l'$ *complex* with $J = 1$ and line strengths between the even-parity $4l4l'$ *complex* with $J = 0$ and the odd-parity $4l5l'$, $4l6l'$ *complexes* with $J = 1$. These calculations are compared with other calculations and with available experimental data. For $Z \geqslant 33$, our data give accurate benchmark values for transition properties of Zn-like ions.

Acknowledgments

The work of MSS was supported in part by National Science Foundation grant no PHY-07-58088.

References

[1] International Committee for Weights and Measures *Proc. of the Sessions of the 95th Meeting (October)* Available at http://www.bipm.org/utils/en/pdf/CIPM2006-EN.pdf
[2] Gorshkov A V, Rey A M, Daley A J, Boyd M M, Ye J, Zoller P and Lukin M D 2009 *Phys. Rev. Lett.* **102** 110503
[3] Safronova M S, Kozlov M G, Johnson W R and Jiang D 2009 *Phys. Rev.* A **80** 012516
[4] Dzuba V A, Flambaum V V and Kozlov M G 1996 *Phys. Rev.* A **54** 3948
[5] Safronova M S and Johnson W R 2007 *Adv. AMO Phys. Ser.* **55** 191
[6] Glowacki L and Migdalek J 2006 *J. Phys. B: At. Mol. Opt. Phys.* **39** 1721
[7] McElroy T and Hibbert A 2005 *Phys. Scr.* **71** 479
[8] Zeng J, Zhao G and Yuan J 2007 *At. Data Nucl. Data Tables* **93** 199
[9] Quinet P, Biémont E, Palmeri P and Träbert E 2007 *At. Data Nucl. Data Tables* **93** 711
[10] Blundell S A, Johnson W R, Safronova M S and Safronova U I 2008 *Phys. Rev.* A **77** 032507
[11] Yu Y J, Li J G, Dong C Z, Ding X B, Fritzsche S and Fricke B 2007 *Eur. Phys. J.* D **44** 51
[12] Jönsson P, Andersson M, Sabel H and Brage T 2006 *J. Phys. B: At. Mol. Opt. Phys.* **39** 1813
[13] Liu Y, Hutton R, Zou Y, Andersson M and Brage T 2006 *J. Phys. B: At. Mol. Opt. Phys.* **39** 3147
[14] Andersson M, Liu Y, Chen C Y, Hutton R, Zou Y and Brage T 2008 *Phys. Rev.* A **78** 062505
[15] Nielsen K, Karlsson H and Wahlgren G M 2000 *Astron. Astrophys.* **363** 815
[16] Andersson M, Jönsson P and Sabel H 2006 *J. Phys. B: At. Mol. Opt. Phys.* **39** 4239
[17] Marques J P, Parente F and Indelicato P 2007 *Eur. Phys. J.* D **41** 457
[18] Andersson M 2009 *Phys. Scr.* T **134** 014021
[19] Andersen T, Nielsen A K and Sørensen G 1973 *Nucl. Instrum. Methods* **110** 143
[20] Luc-Koenig E 1974 *J. Phys. B: At. Mol. Phys.* **7** 1052
[21] Shorer P and Dalgarno A 1977 *Phys. Rev.* A **16** 1502
[22] Knystautas E J and Drouin R 1977 *J. Quantum Spectrosc. Radiat. Transfer* **17** 551
[23] Younger S M and Wiese W L 1978 *Phys. Rev.* A **18** 2366
[24] Hafner P and Schwarz W H E 1978 *J. Phys. B: At. Mol. Phys.* **11** 2975
[25] Fischer C F and Hansen J E 1978 *Phys. Rev.* A **17** 1956
[26] Shorer P 1978 *Phys. Rev.* A **18** 1060
[27] Beck D R and Nicolaides C A 1978 *Phys. Lett.* A **65** 293
[28] Fischer C F and Hansen J E 1979 *Phys. Rev.* A **19** 1819
[29] Younger S M 1980 *J. Quantum Spectrosc. Radiat. Transfer* **23** 489
[30] Beck D R 1981 *Phys. Rev.* A **23** 159
[31] Victor G A and Taylor W R 1983 *At. Data Nucl. Data Tables* **28** 107
[32] Huang K-N and Johnson W R 1985 *Nucl. Instrum. Methods Phys. Res.* B **9** 502
[33] Biémont E, Quinet P and Fawcett B C 1989 *Phys. Scr.* **39** 562
[34] Curtis L J 1989 *J. Phys. B: At. Mol. Opt. Phys.* **22** L267
[35] Hibbert A 1989 *Phys. Scr.* **39** 574
[36] Biémont E 1989 *At. Data Nucl. Data Tables* **43** 163
[37] Migdalek J and Stanek M 1990 *Phys. Rev.* A **41** 2869
[38] Das B P and Idrees M 1990 *Phys. Rev.* A **42** 6900
[39] Cheng T-C and Huang K-N 1992 *Phys. Rev.* A **45** 4367
[40] Chou H-S, Chi H-C and Huang K-N 1994 *Phys. Rev.* A **49** 2394
[41] Martin P, Lavin C and Martín I 1994 *Z. Phys.* D **30** 279
[42] Fleming J and Hibbert A 1995 *Phys. Scr.* **51** 339
[43] Fournier K B 1998 *At. Data Nucl. Data Tables* **68** 1
[44] Meléndez J and Barbuy B 1999 *Astroph. J. Suppl.* **124** 527
[45] Curtis L J 2000 *Phys. Scr.* **62** 31
[46] Safronova U I 2000 *Mol. Phys.* **98** 1213
[47] Bensby T, Feltzing S and Lundström I 2003 *Astron. Astrophys.* **410** 527
[48] Glowacki L and Migdalek J 2003 *J. Phys. B: At. Mol. Opt. Phys.* **36** 3629
[49] Sansonetti J E 2006 *J. Phys. Chem. Ref. Data* **35** 301
[50] Sørensen G 1973 *Phys. Rev.* A **7** 85
[51] Andersen T, Eriksen P, Poulsen O and Ramanujam P S 1979 *Phys. Rev.* A **20** 2621
[52] Denne B, Litzén U and Curtis L J 1979 *Phys. Lett.* A **71** 35
[53] Younger S M, Wiese W L and Knystautas E J 1980 *Phys. Rev.* A **21** 1556
[54] Ansbacher W, Pinnington E H, Bahr J L and Kernahan J A 1985 *Can. J. Phys.* **63** 1330
[55] Migdalek J and Stanek M 1989 *J. Quantum Spectrosc. Radiat. Transfer* **42** 585
[56] Träbert E 1989 *Phys. Scr.* **39** 592
[57] Träbert E, Möller G, Heckmann P H and Livingston A E 1990 *Phys. Scr.* **41** 860

[58] Pinnington E H, Tauheed A, Ansbacher W and Kernahan J A 1991 *J. Opt. Soc. Am.* B **8** 193
[59] Heckmann P H, Möller G, Träbert E, Wagner C, Martinson I, Blanke J H and Sugar J 1991 *Phys. Scr.* **44** 151
[60] Curtis L J 1992 *J. Opt. Soc. Am.* B **9** 5
[61] Hibbert A and Bailie A C 1992 *Phys. Scr.* **45** 565
[62] Träbert E, Heckmann P H, Doerfert J and Granzow J 1993 *Phys. Scr.* **47** 780
[63] Träbert E and Pinnington E H 1993 *Can. J. Phys.* **71** 128
[64] Kernahan J A, Pinnington E H and Träbert E 1995 *Nucl. Instrum. Methods Phys. Res.* B **98** 57
[65] Mishra A P and Balasubramanian T K 2001 *J. Quantum Spectrosc. Radiat. Transfer* **69** 769
[66] Blagoev K B, Malcheva G, Penchev V, Biémont E, Xu H L, Persson A and Svanberg S 2004 *Phys. Scr.* **69** 433
[67] Curtis L J 2007 *J. Phys. B: At. Mol. Opt. Phys.* **40** 3173
[68] Liang L and Zhou C 2008 *J. Quantum Spectrosc. Radiat. Transfer* **109** 1995
[69] Livingston A E 1976 *J. Phys. B: At. Mol. Phys.* **9** L215
[70] Reader J and Luther G 1980 *Phys. Rev. Lett.* **45** 609
[71] Burkhalter P G, Reader J and Cowan R D 1980 *J. Opt. Soc. Am.* **70** 912
[72] Pinnington E H, Bahr J L, Kernahan J A and Irwin D J G 1981 *J. Phys. B: At. Mol. Phys.* **14** 1291
[73] Finkenthal M, Bell R E, Moos H W, Bhatia A K, Marmar E S, Terry J L and Rice J E 1981 *Phys. Lett.* A **82** 123
[74] Bahr J L, Pinnington E H, Kernahan J A and O'Neill J A 1982 *Can. J. Phys.* **60** 1108
[75] Burkhalter P G, Cohen L, Cowan R D and Sweeney B V 1982 *J. Opt. Soc. Am.* **72** 95
[76] Pinnington E H, Bahr J L, Irwin D J G and Kernahan J A 1982 *Nucl. Instrum. Methods* **202** 67
[77] Mandelbaum P, Klapisch M, Bar-Shalom A, Schwob J L and Zigler A 1983 *Phys. Scr.* **27** 39
[78] Litzen U and Reader J 1987 *Phys. Rev.* A **36** 5159
[79] Brown C, Seely J, Kania D, Hammel B, Back C, Lee R, Bar-Shalom A and Behring W 1994 *At. Data Nucl. Data Tables* **58** 203
[80] Churilov S S and Joshi Y N 1995 *Phys. Scr.* **51** 196
[81] Schippers S *et al* 2005 *Nucl. Instrum. Methods Phys. Res.* B **235** 265
[82] Fahy K, Sokell E, O'Sullivan G, Aguilar A, Pomeroy J M, Tan J N and Gillaspy J D 2007 *Phys. Rev.* A **75** 032520
[83] Ralchenko Y, Reader J, Pomeroy J M, Tan J N and Gillaspy J D 2007 *J. Phys. B: At. Mol. Opt. Phys.* **40** 3861
[84] Desclaux J P, Laaksonen L and Pyykko P 1981 *J. Phys. B: At. Mol. Phys.* **14** 419
[85] Chandler G S and Glass R 1987 *J. Phys. B: At. Mol. Phys.* **20** 1
[86] Stiehler J and Hinze J 1995 *J. Phys. B: At. Mol. Opt. Phys.* **28** 4055
[87] Goebel D, Hohm U and Maroulis G 1996 *Phys. Rev.* A **54** 1973
[88] Lundeen S R and Fehrenbach C W 2007 *Phys. Rev.* A **75** 032523
[89] Reshetnikov N, Curtis L J, Brown M S and Irving R E 2008 *Phys. Scr.* **77** 015301
[90] Safronova U I, Johnson W R, Safronova M S and Derevianko A 1999 *Phys. Scr.* **59** 286
[91] Safronova U I, Johnson W R and Berry H G 2000 *Phys. Rev.* A **61** 052503
[92] Safronova U I, Johnson W R, Kato D and Ohtani S 2001 *Phys. Rev.* A **63** 032518
[93] Safronova U I, Johnson W R, Safronova M and Albritton J R 2002 *Phys. Rev.* A **66** 022507
[94] Safronova M S, Johnson W R and Safronova U I 1996 *Phys. Rev.* A **53** 4036
[95] Chen M H, Cheng K T and Johnson W R 1993 *Phys. Rev.* A **47** 3692
[96] Savukov I M and Johnson W R 2000 *Phys. Rev.* A **62** 52512
[97] Safronova U I, Derevianko A, Safronova M S and Johnson W R 1999 *J. Phys. B: At. Mol. Opt. Phys.* **32** 3527
[98] Ralchenko Yu, Jou F-C, Kelleher D E, Kramida A E, Musgrove A, Reader J, Wiese W L and Olsen K 2005 NIST Atomic Spectra Database (version 3.0.2) (Gaithersburg, MD: National Institute of Standards and Technology) Available at http://physics.nist.gov/asd3 (4 January 2006).
[99] Utter S B, Beiersdorfer P and Träbert E 2002 *Can. L. Phys.* **81** 1503
[100] Johnson W R and Huang K-N 1982 *Phys. Rev. Lett.* **48** 315
[101] Huang K-N and Johnson W R 1982 *Phys. Rev.* A **25** 634
[102] Porsev S G, Rakhlina Yu G and Kozlov M G 1999 *Phys. Rev.* A **60** 2781
[103] Safronova M S, Kozlov M G, Johnson W R and Jiang D 2009 *Phys. Rev.* A **80** 012516
[104] Porsev S G and Derevianko A 2006 *J. Exp. Theor. Phys.* **102** 195
[105] Porsev S G, Ludlow A D, Boyd M M and Ye J 2008 *Phys. Rev.* A **78** 032508